Ann. Rev. Fluid Mech. 1986. 18 : 265–305

THE CONTINENTAL-SHELF BOTTOM BOUNDARY LAYER

William D. Grant

Department of Ocean Engineering, Woods Hole Oceanographic Institution, Woods Hole, Massachusetts 02543

Ole S. Madsen

Department of Civil Engineering, Massachusetts Institute of Technology, Cambridge, Massachusetts 02139

INTRODUCTION

Many aspects of the flow of air or water in the vicinity of boundaries have been studied both theoretically and experimentally. Well-known examples occurring in nature include the atmospheric boundary layer, the upper-ocean mixed layer, and shallow-water tidally driven bottom boundary layers. Although the boundary layers for these geophysical flows have many features in common, it has become increasingly obvious that the detailed understanding of each particular type of boundary layer depends on knowledge of the role played by specific processes in determining the boundary-layer scales and the mean and turbulent flow structure.

An important category of geophysical boundary-layer flows is the bottom boundary layer over the continental shelf. The water motion on the shelf is driven by a number of mechanisms, including winds, tides, density differences, atmospheric pressure gradients, and the sea-surface slope. The flow in the boundary layer will contain fluid velocities due to all of these driving mechanisms. The relationship between the boundary-layer characteristics and the externally driven fluid motions is affected by the highly nonlinear friction processes in the boundary layer, and the relationship takes on varying degrees of complexity dependent upon the types of external forcing present. Moreover, the importance of the various driving

0066–4189/86/0115–0265$02.00

mechanisms varies from one continental-shelf region to another and depends on the time scale of the motion one wishes to resolve. Tidal flows dominate some continental-shelf areas, and bottom boundary layers on these shelves fall into a special category because of the importance of acceleration and deceleration on the flow structure. Examples are the Bay of Fundy on the east coast of Canada, Georges Bank on the east coast of the United States, and much of the sea around the British Isles. On most continental shelves, however, a primary forcing for the flow is the alongshore component of wind stress, and in storms, wind forcing is important even on tidally dominated shelves.

Interest in bottom boundary layers stems from a number of their dynamical characteristics. They are regions of turbulent mixing of mass, momentum, and heat. Frictional dissipation of energy takes place in boundary layers, and thus they play an important role in momentum balances. Bottom boundary layers are the interface where exchanges of particles, chemicals, and organisms between seabed and overlying water column take place. The recent focus on continental-shelf boundary layers arises from interest in several contemporary topics in oceanography and engineering.

The first of these topics is understanding wind-driven coastal circulation. It is well known that bottom friction is important to shelf flows, but the actual size of the bottom-friction term is poorly known. Recent work (Smith 1977, Grant & Madsen 1979, Cacchione & Drake 1982, Grant et al. 1984) indicates that the presence of surface waves over rough bottoms results both in a significant increase in the bottom-friction terms over previous estimates and in additional variability of friction across the shelf. Inclusion of a simple model of wave-enhanced friction into a wind-driven shelf circulation model by Clarke & Brink (1985) indicates that this effect is indeed important to the predicted response. In addition, due to the increased bottom friction, the thickness of the bottom boundary layer is considerably larger than previously estimated, and in storms the majority of the water column over the shelf is frictionally dominated. Most models of wind-driven shelf circulation (Allen 1980) assume the surface and bottom layers of frictional influence to be small compared with the water depth; therefore, this assumption needs to be examined.

Another topic, sediment transport on continental shelves, is of practical concern for pollutant transport, for understanding the geological record, and for many engineering applications. More advanced sediment-transport models couple the boundary-layer dynamics to the sediment-transport problem through suspended-sediment and bottom-roughness calculations. Prediction of surface waves in shallow waters is also intricately related to the boundary-layer dynamics through effects of sediment transport and

bottom friction on wave dissipation. It is believed that most of the ocean's biological primary productivity takes place in continental-shelf waters, and the shelf velocity field and mixing are important to this productivity. Recent interest by the biological sciences in the role played by passive deposition versus biological mechanisms in determining the distribution of benthic communities (Hannan 1984), along with interest in feeding mechanisms of various biota, has resulted in the recognition of the potential importance of the role of near-bottom flows and mixing on these biological communities.

Early reviews of the general topic of boundary layers in the ocean were written by Bowden (1962) and Wimbush & Munk (1970). Bowden (1978) and Soulsby (1983) review several types of boundary-layer flows and, in particular, shallow continental-shelf tidal boundary layers. Nowell (1983) provides a review of recent work in oceanic boundary layers. Zeman (1981) reviews general progress in modeling planetary boundary layers, and a review of similarity laws for turbulent wall flows is given by Yaglom (1979). Smith (1977) provides an excellent review of many important aspects of continental-shelf sediment transport. The subject of wind-driven currents on continental shelves has been reviewed by Allen (1980) and Winant (1980). These works, along with others, provide a reasonable picture of our knowledge of oceanic boundary layers and continental-shelf flows in general. While drawing on many aspects of these reviews by pointing out the features shared by all boundary shear flows, we concentrate here on the special features of the continental-shelf wind-driven bottom boundary layer and the associated theoretical, observational, and experimental progress.

To help set the structure within which to review current knowledge on wind-driven continental-shelf bottom boundary layers, we first review some of the important general features of large-scale, quasi-steady, rotating boundary layers (planetary boundary layers) and their oscillatory counterparts (wave boundary layers). These summaries serve to introduce basic definitions of important scales and parameters and their relationships. In the section following these summaries, we describe what is known about the dynamics of the continental-shelf bottom boundary layer and relate this knowledge back to the idealized boundary-layer picture to provide physical interpretations of the basic parameters. The presence of fluid motions covering a wide band of frequencies presents a complex environment in which to make and interpret measurements, and success at these tasks involves careful use of theory and field and laboratory measurements. Some of these problems are reviewed in the last section.

Setting

Figure 1 shows, in schematic form, an idealized picture of the wind-driven continental-shelf bottom boundary layer and surrounding water-column

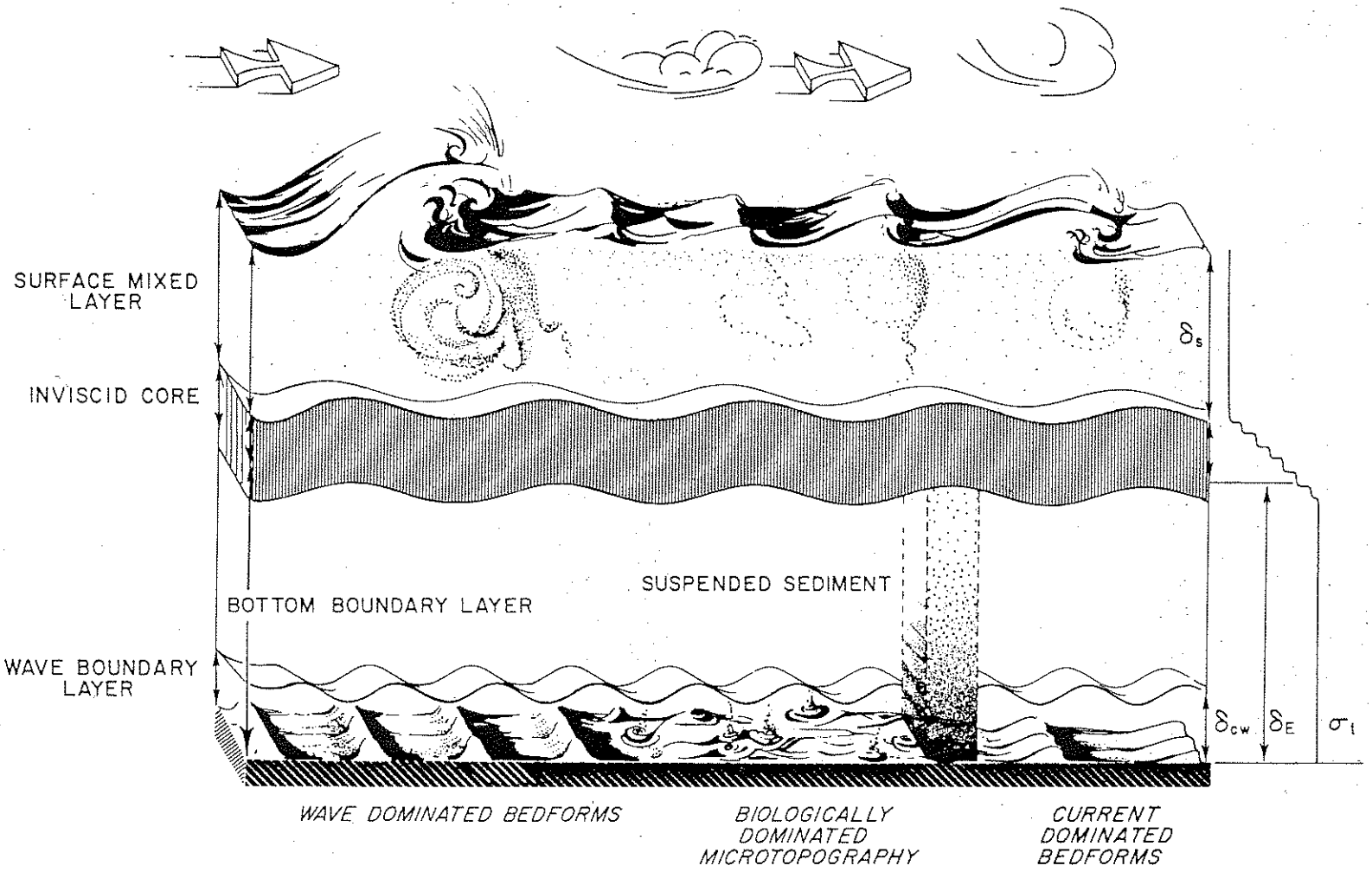

Figure 1 Processes influencing an idealized wind-driven continental-shelf bottom boundary layer, as described in text. The σ_t-profile and boundary-layer scales are indicated.

processes that we describe in this review. When the wind blows over the sea surface it generates both low-frequency water motions (currents) and surface wind waves. In response to the wind forcing, a layer, well mixed in mass, momentum, and heat, develops in the upper ocean; and as the water flows over the seabed, a bottom boundary layer also develops. The surface-wave velocity and pressure fields penetrate to the seabed only in water depths less than about half their wavelength (e.g. Madsen 1976). For example, a 12-s wave, generally in the swell band, will penetrate to the bottom in 112 m of water or shallower, whereas a 6-s wave, typical of the wind-sea band, will penetrate to only 28 m or shallower. Thus, the inner shelf is likely to be influenced by a spectrum of locally generated wind waves and swell, whereas the mid- and outer shelf typically is influenced by a narrow band of swell waves. In storms, the entire shelf can be influenced by locally generated wind waves.

For a bottom shear velocity of 1 cm s^{-1} at a latitude of 40°, the bottom boundary layer would be approximately 40 m thick, neglecting any effects of stratification. A typical surface mixed-layer depth is 20–30 m. In storms with large waves, the estimated neutral bottom boundary-layer thickness can exceed the water depth over most of the shelf, and interaction between the surface layer and the bottom boundary layer can occur. Observations show that considerable vertical density stratification often occurs in the water column, and this stratification plays a major role in determining the surface mixed-layer and bottom boundary-layer thicknesses. Effects of surface-wave breaking can also penetrate substantial distances downward into the water column and may also influence the boundary-layer structure.

Two distinct bottom boundary-layer regions develop under a combined flow of waves and currents. In the immediate vicinity of the bottom, an oscillatory boundary layer exists on the order of 3–5 cm in mild waves and 10–30 cm in strong waves. The wave boundary layer is embedded in a larger planetary boundary layer. Thus, close to the boundary the shear stress and turbulent kinetic energy are due to both waves and currents, whereas above the wave boundary layer these quantities are associated only with the low-frequency flow.

It appears that the vast majority of flows with large waves and currents are hydrodynamically rough because of microtopography generated by biological and sediment-transport processes (i.e. bedforms). Significant amounts of sediment can be put into suspension as a result of wave action. The suspended sediment can modify the density field and result in stratification that, if strong sediment-concentration gradients exist, will influence the near-bottom boundary-layer characteristics just as temperature- and salinity-induced density changes influence the outer boundary-layer region.

THE PLANETARY BOUNDARY LAYER

Equation of Motion and the Mean Velocity Profiles

Boundary layers are typically described in terms of characteristic length and velocity scales that divide the boundary layer into at least two regions: one dependent on the absolute velocity and directly influenced by the boundary, and the other dependent only on the velocity relative to the external driving velocity and the overall scale of the boundary layer. The qualitative description of the mean velocity distribution in the boundary layer can be given in general terms using simple physical arguments and dimensional analysis without dependence on the details of various closure hypotheses (i.e. semiempirical models for turbulence). Such an approach is adopted here to provide basic definitions and scales. For simplicity we consider a very idealized boundary layer and restrict the derivation to geophysical rotating boundary layers that are stationary, horizontally homogeneous, and neutrally stratified, with simple bottom topography and water deeper than the overall vertical scale of the boundary layer. The general framework for the planetary boundary-layer description follows from Blackadar & Tennekes (1968) and Tennekes (1973).

The governing equations for the boundary-layer flow are (Tennekes 1973)

$$-f(u_2-u_{g2})=\frac{\partial \tau_1/\rho}{\partial z}, \tag{1}$$

$$f(u_1-u_{g1})=\frac{\partial \tau_2/\rho}{\partial z}, \tag{2}$$

where u_i $(i=1,2)$ is the mean velocity, τ_i is the shear stress, and f is the Coriolis frequency. Here z is the vertical axis positive upward from the bottom, and the bottom stress is for convenience taken parallel to the x_1 direction.

The usual assumption has been made in simplifying (1) that the pressure gradient is imposed by the external geostrophic velocity, i.e.

$$\begin{aligned} -\frac{1}{\rho}\frac{\partial p}{\partial x_1} &= -fu_{g2}, \\ -\frac{1}{\rho}\frac{\partial p}{\partial x_2} &= fu_{g1}, \end{aligned} \tag{3}$$

where u_{gi} is the geostrophic velocity with magnitude $G=(u_{g1}^2+u_{g2}^2)^{1/2}$, p is the pressure, and ρ is the fluid density.

The relevant dimensional parameters for the mean velocity profile

corresponding to (1) and (2) are the shear velocity $u_* = \sqrt{\tau_b/\rho}$ (where τ_b is the magnitude of the bottom stress), the kinematic viscosity ν, the bottom-roughness length z_0, and ρ, f, and G. Two vertical length scales can be formulated from the dimensional parameters: an overall boundary-layer scale $\delta = u_*/f$ and a viscous length scale $\delta_\nu = \nu/u_*$. The roughness length and ν/u_* are equivalent if the flow is smooth; if the bed is made up of distributed roughness elements, these two scales must be treated independently. We consider here only the case where a single length scale exists near the bed and use z_0 to represent this scale. This simplification does not result in loss of generality for the qualitative features of the flow. It is, however, emphasized that the quantitative specification of z_0 is an essential detail of boundary-layer research.

An external nondimensional parameter governing the flow can be formed, called the surface Rossby number

$$\mathrm{Ro} = \frac{G}{fz_0}. \tag{4}$$

Since the analysis provides a friction law relating G to u_*, the surface Rossby number is seen to implicitly represent a measure of the ratio of the overall boundary-layer scale u_*/f to the roughness length z_0. Thus, the case of practical interest is when $\mathrm{Ro} \gg 1$ and it is clear that $\delta \gg z_0$.

Dimensional analysis leads to the following result for the velocity:

$$u_i(z) = u_* \phi_i\left(\frac{z}{\delta}, \frac{z}{z_0}\right), \qquad i = 1, 2, \tag{5}$$

where ϕ_i is a universal function to be determined. Since $\delta \gg z_0$, the numerical values of z/δ and z/z_0 are very different, and it is physically reasonable to expect that fluid motions near the boundary ($z \ll \delta$) are independent of δ, whereas fluid motions far from the boundary ($z \gg z_0$) are independent of the roughness length z_0. Thus, there exist two bounded limits $\phi_i(z/z_0) = \lim(z/\delta \to 0)$ and $\phi_i(z/\delta) = \lim(z/z_0 \to \infty)$ of $\phi_i(z/z_0, z/\delta)$ (Yaglom 1979).

Two self-similar solutions corresponding to the two bounded limits exist for (1) and (2). The outer limit ($\mathrm{Ro} \to \infty, z/z_0 \to \infty, z/\delta$ finite) corresponds to a velocity-defect law

$$\begin{aligned} \frac{u_1 - u_{g1}}{u_*} &= \phi_1(z/\delta), \\ \frac{u_2 - u_{g2}}{u_*} &= \phi_2(z/\delta). \end{aligned} \tag{6}$$

The inner limit ($\mathrm{Ro} \to \infty, z/\delta \to 0, z/z_0$ finite) corresponds asymptotically

to a constant-stress layer (Blackadar & Tennekes 1968) and is written as

$$\frac{u_1}{u_*} = \phi_1(z/z_0),$$
$$\frac{u_2}{u_*} = 0, \tag{7}$$

where the second identity results from the convention that the stress is aligned with the x_1-axis.

At this point no statement has been made about the shape of the velocity profiles in each region: Only their dependence on two different length scales has been considered. The actual form of the velocity profiles can be found by assuming that there exists an overlap layer, $z_0 \ll z \ll \delta$, in which both (6) and (7) are valid simultaneously (Clauser 1956, Yaglom 1979). It follows from equating the derivatives of (6) and (7) within this overlap layer that both functions are logarithmic:

$$\frac{u_1 - u_{g1}}{u_*} = A \ln(z/\delta) + B, \tag{8}$$

$$\frac{u_1}{u_*} = A \ln(z/z_0). \tag{9}$$

In the limit $\mathrm{Ro} \to \infty$, A is equal to a universal constant, where $1/A$ is called the von Kármán constant κ. There has been considerable debate over the actual value of κ and its variability (e.g. Yaglom 1979) with smooth or rough terrain (Tennekes 1973), with $\mathrm{Re}_* = u_*\delta/\nu$ (e.g. Huffman & Bradshaw 1972), and with suspended-sediment load (e.g. Coleman 1981, 1984). The most recent results indicate that $\kappa = 0.40$ or 0.41 is a reasonable value for fully turbulent, rough flows.

The value of the constant B is less well known. Tennekes (1973) gives the average value of κB as approximately 1 (i.e. $B = 2.5$ with $\kappa = 0.4$) for atmospheric boundary layers. Yaglom (1979) suggests that B is slightly above 2 (with a mean of about 2.35 for all suggested values) in boundary-layer flows. For oceanic boundary layers, no direct determinations of the values of B have been reported. The value of B will be sensitive to κ and to the scale height used for the boundary layer. Equation (8) is in principle unbounded and is valid only for $z < \delta_E$, the Ekman-layer thickness. Limiting the values of z for which (8) is valid to $u_1 \leq u_{g1}$ gives $\delta_E \simeq 0.4\delta = 0.4u_*/f$, which is in reasonable agreement with limited observational evidence for neutral boundary layers.

In spite of the simplicity of the analysis above, a number of concepts of major importance to understanding continental-shelf boundary-layer behavior follow from it. In particular, it is important to examine the

significance of the existence of a region of logarithmic velocity near the boundary, its dependence on the roughness length scale, and the meaning of this length scale; the relationship between the external geostrophic flow and bottom friction; and the idea of a constant-stress layer and its relationship to the logarithmic layer.

Logarithmic Velocity Region

Equation (9) shows that there is a region where z/z_0 is finite but $z/\delta \ll 1$, within which the velocity distribution is described by a logarithmic function. The argument of this function depends on the roughness length z_0. This result depends only on the existence of an overlap layer in z, where $z_0 \ll z \ll \delta$, and requires no assumptions on the closure used to solve (1) and (2), on the existence of a constant-stress layer, or on the nature of the flow in the region $z/z_0 \to 0$. The theory cannot provide any quantitative value for the scale of the log layer; it only states that z/z_0 is finite. Furthermore, the physical cause(s) of the roughness length is not specified, nor is the actual range of magnitudes of z_0. Discussion of the concept of roughness length is deferred to a later section.

The overlap layer is the transition region between two regions described by different physical scales: the overall boundary-layer scale δ, and the roughness scale z_0. Many geophysical flows exist where there are more than two length scales to consider. The existence of the log or log-deficit velocity profiles is not guaranteed for such flows, and the actual profile will depend on the size of the scales of importance for the other processes relative to the roughness length and the overall boundary-layer scale. Examples of flows with additional length scales are accelerated and decelerated flows, flows over topographic features, stratified flows, and unsteady oscillatory flows involving an internal boundary-layer scale. Yaglom (1979) gives a general discussion of flows subject to pressure gradients, and specific cases for stratified and oscillatory flows are described below. Once the appropriate physical length scales are identified, the general analysis can be carried out as described, for example, in Yaglom (1979). Each general dimensional analysis results in unknown constants and functions that can be evaluated using both dynamical equations and data for the flow of interest. For large-scale rotating boundary layers, very few data for the overall boundary-layer scale exist, and presently one is forced to resort to largely unproven results obtained by solving the dynamical equation using some type of closure.

Drag Law

It is of interest to relate the external geostrophic flow, which is in theory easily measured, to the internal friction velocity, which is generally assumed unknown. The open-channel and pipe-flow analogues to this problem are

skin-friction laws (e.g. Clauser 1956) that allow the friction velocity and external-flow velocity to be used interchangeably.

Since (8) and (9) are simultaneously valid within the overlap layer, they can be equated at a point within this layer to yield

$$\frac{u_{g1}}{u_*} = \frac{1}{\kappa} \ln\left(\frac{\delta}{z_0}\right) - B \tag{10}$$

and $u_{g2}/u_* = -C/\kappa$ (Blackadar & Tennekes 1968).

If the geostrophic velocity is known along with f, z_0, and the constants B and C, the shear velocity can in principle be computed. Defining a geostrophic drag coefficient f_g by $u_*/G = (f_g/2)^{1/2}$ and substituting $G \simeq u_{gi}$ with u_{g1} from (10), an approximate expression for the drag coefficient in terms of the surface Rossby number is obtained:

$$\frac{1}{4\sqrt{f_g}} + \log\frac{1}{4\sqrt{f_g}} = \log\left(\frac{G}{fz_0}\right) - 1.19. \tag{11}$$

The limitations to applying this procedure in practice are primarily due to the assumptions of neutral, stationary flow. In storm-driven flows, no geostrophic balance may exist because of turbulent mixing from both the surface and bottom, and G may be difficult to define.

Constant-Stress Layer

No constant-stress assumption was required to derive the general form of the velocity profiles. The actual stress profile is easily derived by substituting the solutions for u_1, u_2, u_{g1}, and u_{g2} into the governing equations and then integrating. Adopting the results of Tennekes (1973), where $z/z_0 \gg 1$ has been used to simplify the result, the nondimensional stress profile in the overlap region is given as

$$\frac{\tau_1/\rho}{u_*^2} = 1 - \frac{C}{\kappa}\frac{z}{\delta}, \tag{12}$$

$$\frac{\tau_2/\rho}{u_*^2} = \frac{z}{\delta}\left\{\frac{1}{\kappa}\left[\ln\left(\frac{z}{\delta}\right) - 1\right] + B\right\}. \tag{13}$$

Tennekes takes typical values for C equal to 5 and κB equal to 1. Laboratory results (Clauser 1956) indicate that the logarithmic velocity layer holds up to approximately 10% of the boundary-layer thickness. The neutral boundary-layer thickness is generally taken as 0.4δ, so the log layer is 0.04δ. Using these estimates in (12) and (13) shows that the magnitude of the stress has decreased by up to 40% and the stress has turned by over 30° at the top of the log layer.

The conclusion from this result is important. The log-profile approximation is accurate to a much greater level in the boundary layer than the approximation of constant-stress layer. This point is well supported by observations in natural flows. In fact, the stress is within 1% of its value at the boundary only for $z/\delta < 10^{-3}$. For a 40 m thick boundary layer this height corresponds to less than 10 cm. The logarithmic or overlap layer is only a constant-stress layer in an asymptotic sense as $z/\delta \to 0$ for $\mathrm{Ro} \gg 1$.

THE WAVE BOUNDARY LAYER

It was noted in the introduction that for the general case of interest on the shelf, the fluid motions at the seabed are due to both surface waves and currents. This situation is considered in the following section, but it is first worthwhile to describe the characteristics of the boundary layer under pure waves.

The linearized momentum equation governing the oscillatory flow under the wave in the immediate vicinity of the boundary is

$$\frac{\partial \tilde{u}}{\partial t} = -\frac{1}{\rho}\frac{\partial \tilde{p}}{\partial x} + \frac{\partial \tau/\rho}{\partial z}, \tag{14}$$

where the wave, for simplicity, is assumed to propagate in the x-direction. The assumptions behind (14) and their implications are discussed in Grant & Madsen (1979) and Trowbridge & Madsen (1984a). The usual boundary-layer assumption that the pressure gradient is imposed by the external potential flow $\tilde{u}_\infty$ is invoked, and (14) becomes

$$\frac{\partial(\tilde{u}-\tilde{u}_\infty)}{\partial t} = \frac{\partial \tau/\rho}{\partial z}. \tag{15}$$

It is interesting to note the similarity (Madsen 1977) between (15) for a simple harmonic motion ($\partial/\partial t = i\omega$) and (1) and (2). In fact, the radian frequency ω plays the same role in (15) as does f in (1) and (2), while $u_b = |\tilde{u}_\infty|$ replaces G. Jonsson (1980) finds wave boundary layers to be turbulent for $u_b^2/\omega\nu > 1 \times 10^5$, and thus most wave boundary-layer flows of interest on the continental shelf are turbulent. The wave boundary-layer thickness is then, by analogy, proportional to u_{*w}/ω, in which u_{*w} is a representative shear velocity for the wave boundary-layer flow. Coriolis force has no significant influence on the thin wave boundary-layer flow, and the nondimensional external parameter $u_b/\omega z_0$ for the wave boundary layer is physically equivalent to the surface Rossby number. Two self-similar solutions to (15) can be found. In the immediate vicinity of the boundary ($z/z_0 \to 0$), unsteadiness vanishes ($\tilde{u} \to 0$) and the solution to (15) is a quasi-

steady law-of-the-wall. The logarithmic velocity region depends on the roughness length z_0 and requires the presence of an overlap layer in z, where $z_0 \ll z \ll \delta_w$, to exist. Thus, for a log profile to exist, the roughness length must be small relative to the wave boundary-layer thickness δ_w.

The external-flow velocity and the boundary shear stress can be related through a wave friction factor analogous to the drag law for the quasi-steady planetary boundary layer. Thus, we define $u_{*w}/u_b = \sqrt{f_w/2}$, (where f_w is the wave friction factor) and $u_{*w} = \sqrt{\tau_w/\rho}$ (where τ_w is the maximum bottom shear stress). Several expressions have been developed for the wave friction factor, starting with the pioneering work of Jonsson (1966). Assuming the velocity profile to be logarithmic throughout the entire wave boundary layer, Jonsson (1966) derived an expression for f_w with a single constant that was determined from a laboratory experiment. Kajiura (1964, 1968) and Grant (1977) derived theoretical expressions for the wave friction factor, assuming an eddy-viscosity closure for the dynamical equation. Kamphuis (1975) derived expressions for the wave friction factor from a series of laboratory experiments. Recent theoretical work by Trowbridge & Madsen (1984a) has used more realistic eddy-viscosity models to derive expressions for the wave friction factor. Encouragingly, these expressions give similar predictions (e.g. Grant 1977, Trowbridge & Madsen 1984a), and the minor differences can be attributed to the closure used or the definition of bottom roughness. These expressions have the identical form to (11) for the geostrophic drag coefficient, with a different constant on the right-hand side (-1.8, Grant; -1.56, Jonsson) and the parameter G/fz_0 replaced by $u_b/\omega z_0$. This analogy also illustrates that $f_w \gg f_g$ (since $\omega \gg f$) and explains why wave-induced shear stresses are much larger than current-induced stresses for comparable bottom roughness and velocities ($u_b \simeq G$).

Quantitative derivations of the actual form of the velocity profile within the wave boundary layer and the variation in boundary shear stress also depend on the closure used to solve (15). The treatment of the wave boundary layer in combined wave and current flows is based on an analogy with models for the pure-wave case, since few data inside the wave boundary layer are available for the combined-flow case. Therefore, we review several general conclusions about the effect of various closure assumptions on the predicted wave boundary-layer behavior.

For the planetary boundary layer, the stress distribution was shown to be a constant in the limit $z/\delta \to 0$. A similar analysis can be carried out for the wave boundary layer, provided that $u_b/\omega z_0 \to \infty$. Similarly, the logarithmic velocity law can be shown to be valid for $z_0 \ll z \ll \delta_w$. As a consequence of these two results, an eddy viscosity ν_T can be derived (e.g. see Tennekes

1973),

$$\nu_T = \frac{u_*^2}{|d\tilde{u}/dz|} = \kappa u_* z, \tag{16}$$

which is valid very near the boundary. Scaling the turbulent kinetic-energy equation shows the balance between production and dissipation to be quasi-steady near the boundary (Trowbridge 1983). This result, together with (16), indicates a reasonable eddy viscosity to be linearly varying with z while scaled by the instantaneous shear velocity. The importance of time variability in the eddy-viscosity model has been addressed by Lavelle & Mofjeld (1983) and Trowbridge & Madsen (1984a,b). The Trowbridge & Madsen (1984a,b) results demonstrate that the first-order solution depends only slightly on time variation in the eddy viscosity and is more sensitive to the proper treatment of vertical variability. However, at second order in wave steepness, Trowbridge & Madsen (1984b) show that including time variability in the eddy viscosity becomes extremely important.

If we adopt the form of the eddy viscosity given in (16) (with $u_* = u_{*w}$) to represent the stress term in (15), assume a periodic wave motion specified by its near-bottom orbital velocity $\tilde{u}_\infty = u_b \exp(i\omega t)$, and apply the usual no-slip boundary condition $\tilde{u} = 0$ at $z = z_0$, the solution for the velocity within the wave boundary layer is (Grant 1977)

$$\tilde{u} = \left(\frac{\ker 2\sqrt{\zeta} + i \operatorname{kei} 2\sqrt{\zeta}}{\ker 2\sqrt{\zeta_0} + i \operatorname{kei} 2\sqrt{\zeta_0}} \right) u_b e^{i\omega t}, \tag{17}$$

where ker and kei are the Kelvin functions of zeroth order, and ζ is the nondimensional vertical boundary-layer coordinate defined by $\zeta = z/\ell$ with $\ell = \kappa u_{*w}/\omega$, and $\zeta_0 = z_0/\ell$.

For small values of ζ and ζ_0, the asymptotic expressions for the Kelvin function (Abramowitz & Stegun 1972, pp. 379–85) may be used to simplify (17) to the classical logarithmic velocity profile

$$|\tilde{u}| = \frac{u_b}{\left[(\ln \zeta_0 + 1.15)^2 + \left(\frac{\pi}{2} \right)^2 \right]^{1/2}} \ln (z/z_0). \tag{18}$$

Thus, the result expected from similarity theory is recovered. The logarithmic approximation is found to be valid for $z < 0.1\delta_w$ (Grant 1977), in agreement with results quoted for planetary boundary layers.

The solution given by (17) is complex and can be represented by a velocity magnitude and phase between the external potential-flow velocity and the boundary-layer velocity. When the results of the simple model are tested

against the laboratory experiments of Jonsson & Carlsen (1976), the predicted and experimental velocity magnitudes show good agreement overall, with excellent agreement in the lower part of the logarithmic layer and about a 4% overprediction of the model in the region of overshoot in the velocity profile. The phase is not well predicted. Physically, the eddy viscosity cannot increase through the entire boundary layer, as is assumed in (16). More realistic eddy-viscosity models employ either an exponentially decaying (Long 1981, Sanford 1984) or constant eddy viscosity (Kajiura 1967, Brevik 1981) in the outer part of the boundary layer and show very good agreement with both the velocity magnitude in the overshoot region and the phase. Figure 2 shows a comparison between the laboratory results of Jonsson & Carlsen (1976) and model results solving (15) with (*a*) the simple time-invariant, linearly varying, eddy-viscosity closure presented here and (*b*) the exponential eddy-viscosity model from Sanford (1984). The phase shift between the external flow and the boundary-layer flow in an oscillatory boundary layer is analogous to the turning angle in the planetary boundary layer and is known to depend strongly on the closure scheme, so the result above is not surprising.

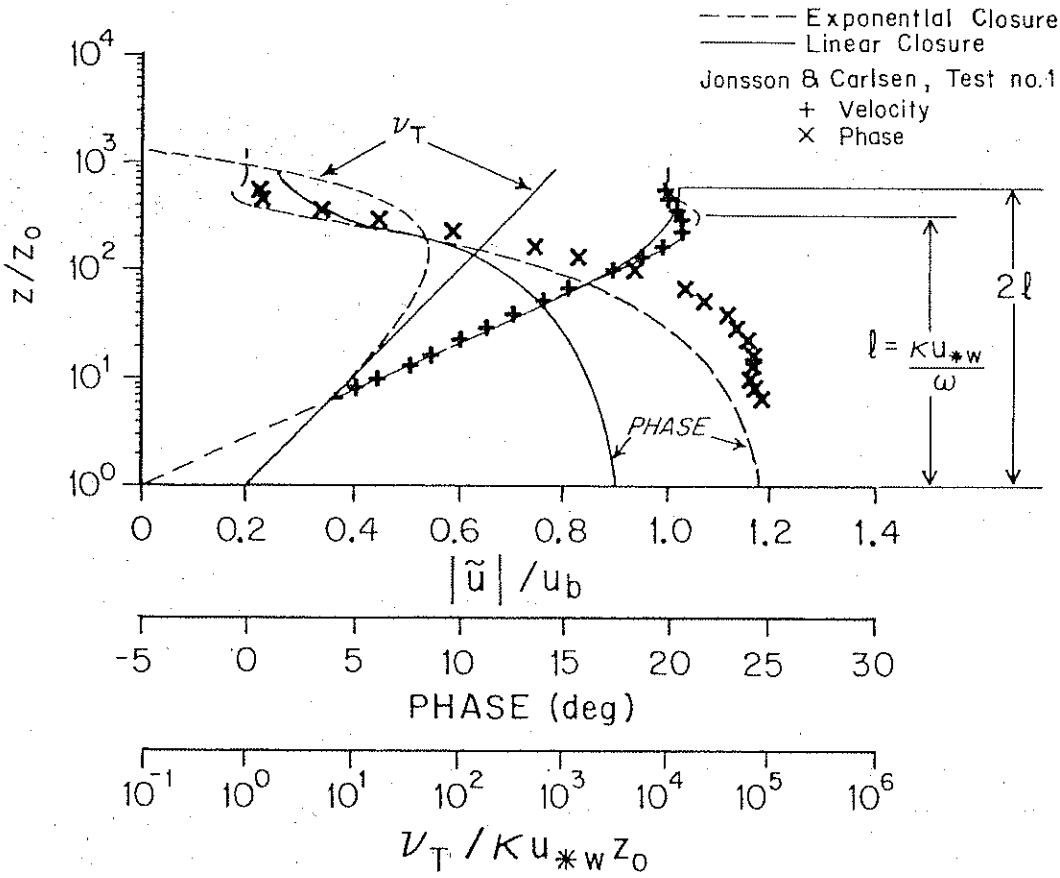

Figure 2 Comparison of pure-wave boundary-layer velocity magnitude and phase from two different models with experimental data. Eddy viscosities for each model are also plotted.

THE WAVE-CURRENT BOUNDARY LAYER

The simultaneous presence of low-frequency current and surface-wave velocity components in natural flow over a *hydrodynamically rough bottom* results in a nonlinear interaction that modifies both flows and the associated boundary shear stress. Scaling arguments presented in the discussions of wave and planetary boundary layers demonstrate that two distinct vertical boundary-layer scales exist for this combined-flow situation; in the immediate vicinity of the bottom, a wave boundary layer develops that is embedded in a large-scale rotating boundary layer. In the wave boundary layer, both waves and currents contribute to the turbulence. The height $\delta_{cw} = \kappa u_{*cw}/\omega$ (where the subscript cw denotes both wave and current contributions to the shear velocity) to which the wave-induced turbulence can diffuse limits the region of wave turbulence to the wave boundary layer; above this region, the turbulence is associated with the low-frequency current only. The third vertical length scale of importance to the problem, the roughness scale z_0, is limited to values $z_0 \ll \delta_{cw}$.

Combined wave and current flows have only recently been studied in detail, and much of what is known about the mechanism of wave-current interaction is based on models. The first rational treatment of such flows was by Lundgren (1972), who developed a simple model for the current in the presence of a wave for codirectional and perpendicular flows. Lundgren (1972) noted the difference in the boundary-layer scales, but treated only the current and did not include nonlinear interaction. The first models to hypothesize the nonlinear-interaction mechanism and to treat the flow for both the wave and the current in both boundary-layer regions simultaneously were developed by Grant (1977) and Smith (1977) [see also Grant & Madsen 1979 (hereafter, along with Grant 1977, referred to as GM)]. Both these models concentrated on the near-bottom flow and used simple time-invariant, linearly varying eddy-viscosity closures to model the flow while adopting different velocity scales in their closures. Other models are referenced by Trowbridge & Madsen (1984a). Only the GM model was formulated in a general way to treat waves and currents at arbitrary angles. Both Smith and GM have since developed more complete full boundary-layer models (see Grant & Glenn 1983, Paradis 1983, Sanford 1984, Wiberg & Smith 1983) that also treat other geophysically important effects (e.g. movable bed roughness, stratification, internal waves). In spite of more physically realistic closures and better treatment of time variability (see comments on wave boundary-layer modeling closures), the important physical effects of the combined wave and current theories are reasonably represented in these earlier models.

To help illustrate the important physics that all wave-current models

must include and the implication of these physics, a simplified model is presented here. For the combined wave and current flow, straightforward analytical solutions to (14) follow if we adopt a simple time-invariant eddy viscosity increasing linearly with z. Close to the boundary ($z < \delta_{cw}$), the eddy viscosity is scaled with the combined wave-current shear velocity, which for simplicity is chosen as the maximum shear velocity $u_{*cw} = \sqrt{\tau_{cw}/\rho}$ (see arguments in GM; Smith 1977). For $z > \delta_{cw}$, but still within the near-constant-stress layer of the current, the velocity scale for the eddy viscosity is $u_{*c} = \sqrt{\tau_c/\rho}$, based on the mean bottom stress τ_c. The resulting shear-stress model is

$$\tau_i = \rho \nu_T \frac{\partial u_i}{\partial z}, \tag{19}$$

with

$$\nu_T = \begin{cases} \kappa u_{*cw} z, & z < \delta_{cw}, \\ \kappa u_{*c} z, & z > \delta_{cw}. \end{cases} \tag{20}$$

Substitution of (19) and (20) into (14) leads to an equation that may be split into parts governing the wave motion and the *near-bottom* current. The reader is referred to GM for details. The solution for the wave motion for $z < \delta_{cw}$ is identical to the pure-wave case except that u_{*w} now is replaced by u_{*cw} in the definition of $\ell = \kappa u_{*cw}/\omega$.

Since ℓ is the scale of the wave boundary-layer thickness, it follows that $\zeta_0 \ll 1$, where ζ_0 is the roughness parameter. For small values of ζ and ζ_0, the asymptotic expressions for the Kelvin functions (Abramowitz & Stegun 1972, pp. 379–85) may be introduced, and the classical logarithmic profile (18) is obtained. From (18), (19), and (20) the maximum wave bottom shear stress τ_{wm} is obtained:

$$u_{*wm}^2 = \tau_{wm}/\rho = \frac{\kappa u_{*cw} u_b}{\left\{\left[\ln\left(\frac{\kappa u_{*cw}}{z_0 \omega}\right) - 1.15\right]^2 + \left(\frac{\pi}{2}\right)^2\right\}^{1/2}}; \tag{21}$$

this expression shows that the current affects the wave stress through u_{*cw}. Vector addition of the enhanced stress components results in an expression for u_{*cw}:

$$u_{*cw} = u_{*wm}[1 + 2(u_{*c}/u_{*wm})^2 \cos\phi + (u_{*c}/u_{*wm})^4]^{1/4} = \sqrt{C_R}\, u_{*wm}, \tag{22}$$

where ϕ $[0 \le \phi \le \pi/2]$ denotes the angle between waves and current. For large wave stresses relative to the current stress (i.e. $u_{*c} < u_{*wm}$), as is commonly encountered on continental shelves, the coefficient C_R is

expected to be only slightly larger than unity. This inferred similarity between waves in the presence and absence of currents can be exploited by defining a generalized wave friction factor through

$$u_{*wm} = \sqrt{\tau_{wm}/\rho} = \sqrt{C_R}\,\sqrt{f_w/2}\,u_b. \tag{23}$$

With (22) and (23) an approximate wave-friction-factor relationship,

$$\frac{1}{4\sqrt{f_w}} + \log\frac{1}{4\sqrt{f_w}} = \log\left(\frac{C_R u_b}{\omega z_0}\right) - 1.65 + 0.24\,(4\sqrt{f_w}), \tag{24}$$

is obtained from (21). Realizing that this relationship, by virtue of $\zeta_0 \ll 1$, is limited to values of $u_b/\omega z_0 > 300$, we note that it is for practical purposes equivalent to the semiempirical relationship obtained by Jonsson (1966) for a pure wave motion ($C_R = 1$). Note again the analogous form to the geostrophic drag coefficient, (11). The last term on the right-hand side of (24) is absent in (11) by virtue of the approximation $u_{g1} \simeq G$, made in the derivation of (11). The difference in the constant (-1.65 as opposed to -1.19) in the two equations is due to the inclusion of κ in the definition of the wave-boundary-layer length scale ($\ell = \kappa u_{*cw}/\omega$), while $\delta = u_*/f$ was adopted for the planetary boundary layer. The implicit relationship for f_w given by (22), (23), and (24) is readily solved iteratively from knowledge of u_b, ω, z_0, and u_{*c} by initially assuming $C_R = 1$ in (23) and (24) and subsequently obtaining an improved estimate of C_R from (22), with which the procedure is repeated.

The equations governing the near-bottom current are solved (see GM) subject to the no-slip boundary conditions $z = z_0$ for $z < \delta_{cw}$ and $z = z_{0c}$ for $z > \delta_{cw}$ and yield the current profiles

$$u_c = \begin{cases} \dfrac{u_{*c}}{\kappa}\left(\dfrac{u_{*c}}{u_{*cw}}\right)\ln\dfrac{z}{z_0}, & z \le \delta_{cw}, \\ \dfrac{u_{*c}}{\kappa}\ln\dfrac{z}{z_{0c}}, & z \ge \delta_{cw}, \end{cases} \tag{25}$$

in which z_{0c} is the *apparent roughness* experienced by the current in the presence of waves, i.e. the roughness determined from a log-profile analysis of current observations obtained outside the wave boundary layer. This second solution is now equivalent to the log layer for the planetary boundary layer, i.e. z_{0c} and *not* z_0 is the appropriate roughness for the planetary boundary layer in the presence of waves.

The solution for the "mean" velocity profile inside the wave boundary layer is seen to depend on the physical bottom roughness and has a shear velocity that is modified by the term (u_{*c}/u_{*cw}) expressing the effect of the nonlinear wave-current interaction. This term indicates that the slope of the

velocity profile inside the wave boundary layer would not correspond to the mean shear velocity in a usual semi-log velocity plot; moreover, as the strength of the wave increases relative to the current, the effective shear velocity will also increase.

By matching the current from each boundary layer at $z = \delta_{cw}$, an alternative expression,

$$u_c = \frac{u_{*c}}{\kappa}\left(\frac{u_{*c}}{u_{*cw}} \ln \frac{\delta_{cw}}{z_0} + \ln \frac{z}{\delta_{cw}}\right), \tag{26}$$

is obtained for $z > \delta_{cw}$. It is noted that (26) in the limit $u_{*c} \to u_{*cw}$ (i.e. negligible wave contribution) reduces to the rough turbulent profile specified by z_0; $u_{*c} \ll u_{*cw}$ yields a profile corresponding to an apparent roughness related to the wave-boundary-layer thickness ($\delta_{cw} \gg z_0$). This latter observation underscores that the effect of waves on the near-bottom current profile may be appreciable.

To render (26) predictive, it is necessary to specify the value of δ_{cw}, which scales with ℓ, where the current is matched. The effect of ambiguity in the choice of δ_{cw} should be considered together with the uncertainty associated with estimating z_0. Although predictive relationships for the roughness of a movable bed, discussed in the next section, have been proposed, the *prediction* of z_0 presently contains considerable uncertainty. If we neglect the implicit dependency of u_{*cw} on z_0, the error associated with knowledge of δ_{cw} and z_0 within factors of ε_δ and ε_N, respectively, is $\pm(1 - u_{*c}/u_{*cw}) \ln \varepsilon_\delta$ $\pm(u_{*c}/u_{*cw}) \ln \varepsilon_N$. For values of $u_{*c}/u_{*cw} > 1/3$, an error in δ_{cw} by a factor of $\varepsilon_\delta = 2$ is significant only if the bottom roughness is known better than within a factor of 4. For smaller values of u_{*c}/u_{*cw} when the magnitude of the current is small, other effects not accounted for [e.g. wave-induced mass transport (Trowbridge & Madsen 1984b)] may come into play. From a practical point of view, the ambiguity in the choice of δ_{cw} is therefore presently overshadowed by our incomplete ability to predict the bottom roughness z_0 and to account for other processes influencing the wave boundary layer.

From considerations of the distance required for (17) to approach the free-stream velocity, a value of $\delta_{cw} = 2\ell$ was suggested by GM, while the comparison of the linear wave model of Trowbridge & Madsen (1984a) with the data of Jonsson & Carlsen (1976) suggests a value of $\delta_{cw} = \ell$ (see also Figure 2). Both of these analyses use a boundary-layer definition based on a percentage of the free-stream velocity. The use of other criteria based on, for example, stress or stress divergence will give other relationships between δ_{cw} and ℓ. Until accurate experimental data for waves and currents corresponding to the range of validity of the simple model presented here

(i.e. rough turbulent flow and $u_b/\omega z_0 > 300$) become available, a choice $\delta_{cw} \simeq (1\text{–}2)\ell$ is recommended. The problem of specifying δ_{cw} to make (26) predictive may be avoided by using a continuous eddy-viscosity formulation (e.g. Wiberg & Smith 1983, Sanford 1984). However, the problem is transferred to the choice of an appropriate scale height in the eddy-viscosity formulation, and the same comments on the uncertainty of the prediction relative to z_0 are relevant.

The solution of the "wave problem" from given values of u_b, ω, z_0, and u_{*c} was discussed above. The current profile is predicted directly from (26) with $\delta_{cw} = (1\text{–}2)\ell$. It is evident that the magnitude of the current velocity corresponding to a given value of u_{*c} decreases as the wave motion, and hence u_{*cw} and δ_{cw}, increases. A more typical problem specification would be that u_c is known at a given elevation $z = z_r > \delta_{zw}$ above the bottom rather than u_{*c}. For this case an initial estimate $u_{*cw} = u_{*wm}$ is obtained from (23) and (24) with $C_R = 1$, and (26), which is quadratic in u_{*c}, may be solved for u_{*c}. With this estimate of u_{*c}, a value of C_R may be obtained from (22) and the procedure may be repeated. It is evident that the predicted average bottom shear stress experienced by a current of a given magnitude increases with increasing wave motion.

BOTTOM ROUGHNESS

The description of the dominant hydrodynamic elements of the bottom boundary layer on wind-driven continental shelves has identified the importance of the bottom roughness length scale z_0. Normally, the flow over a boundary covered with roughness elements of some geometrical scale is considered when defining the roughness length scale. The mean velocity near the wall can be written in the general form

$$u = u_* f\left(\frac{z-d_*}{k}, \frac{ku_*}{\nu}, \frac{l_1}{k}, \frac{l_2}{k}, \ldots\right), \tag{27}$$

where k is the mean height of the roughness elements, l_1, l_2, etc., are the other geometrical length scales defining the geometry of the roughness elements, d_* is the displacement height, and $z = 0$ at the level from which the roughness elements protrude into the flow. For natural bottoms the level $z = 0$ is quite ambiguous, and $z - d_*$ may be thought of as defining the theoretical bed location. The parameter z_0/k is then a function of ku_*/ν, l_1/k, etc., and the expression given in (27) results in the usual logarithmic velocity profile. The details of this derivation, along with discussions of the relationship between z_0 and the geometry of the boundary roughness represented by l_1, can be found in Wooding et al. (1973), Yaglom (1979), and Jackson (1981).

At least three distinct types of roughness configurations exist, each with its own scaling law as summarized in Table 1. Jackson (1981) studied d_* and established an empirical expression $d_* = 0.7z_0$ applicable to a range of roughness configurations. Businger (1974), Yaglom (1979), and Jackson (1981) provide physical interpretations of z_0 and d_* and their relation to roughness geometry. The physical interpretations are that z_0 represents the magnitude of the forces acting on the boundary surface, whereas d_* represents the distribution of these forces. This very general physical interpretation of z_0, as related to the magnitude of the forces felt at the base of the wall layer and not to the causes of the forces (i.e. geometry or wave effects), has important implications in the understanding of roughness lengths for continental-shelf flows.

The effects of many of the phenomena influencing the continental-shelf boundary-layer flow are intricately linked to the presence of other phenomena. We have seen that waves can affect the boundary roughness experienced by the planetary boundary-layer flow (z_{0c} as opposed to z_0) as a result of the increased bottom shear stress and hence near-bottom turbulent intensity associated with the wave-boundary-layer flow. Since the bottom of most continental shelves consists of movable sediments that respond to the forces (the shear stress) exerted by the flow, waves also play a significant role in the formation of bottom features and bedforms.

Bedforms are characterized by their height and the spacing between crests, the ratio of which is called steepness. Classification of bedforms vary, but typically they fall into ripples, dunes, and sand waves, with a range of

Table 1 Summary of geometrical roughness types

Roughness type	Characteristics	Scaling law
"k" (Perry et al. 1969)	Spacing of elements equal to height or less; unstable eddies form behind each element.	$z_0 \propto k$
"δ" (Perry et al. 1969)	Spacing between elements small relative to element width; stable eddy forms between elements; skimming flow.	$z_0 \propto \nu/u_*, \delta$
"k, δ" (Wooding et al. 1973)	Spacing between elements, l, large relative to separation region behind; separated flow reattaches between elements.	$z_0 \propto k, l$

heights from several millimeters to meters and of spacing from centimeters to tens of meters (Allen 1968). When the bed features become large relative to the boundary-layer scales, they no longer act as roughness elements but rather as topographic steering mechanisms for the flow.

A range of scales of bed features can exist simultaneously (e.g. small-scale ripples superposed on large sand waves). Smith & McLean (1977a) developed a model to describe the spatially averaged flow over such features. Their model treats the flow by identifying local roughness scales, each corresponding to a velocity region based on the hypothesized existence of an overlap layer such that $z_{0i} \ll z_{0i+1}$ in the ith layer, and the local roughness in each region depends on the roughness in the regions below. The velocity profile over multiple roughnesses is therefore made up of segmented quasi-logarithmic-profile regions. Smith & McLean's (1977a,b) model was developed for unidirectional flows, but the general approach is applicable to most continental-shelf regions, even with tidal flows, if one accounts for the fact that the smaller-scale bedform can change with the change in the local boundary shear stress.

High near-bed transport rates in quasi-steady flows are hypothesized to affect z_0. Smith & McLean (1977a,b) developed a simple model to predict this roughness using an analogy with the work of Owen (1964) for eolian transport. In Smith & McLean's model, the bed-load roughness is expressed as $z_0 = \alpha_0(u_*^2 - u_{*cr}^2)/g(s-1)$, where α_0 is a constant, $s\,(=\rho_s/\rho)$ is the relative sediment density, u_{*cr} is the critical shear velocity, and g is the acceleration of gravity. The constant α_0 was found to equal 26.3 for the Columbia River data used by Smith & McLean (1977a,b). For low sediment-transport rates, Dyer (1980) found agreement with the above formula, while bedform conditions dominated the z_0 value during high flows and it was unclear if the bed-load roughness was still predicted accurately.

Surface-Wave Effects on Bottom Roughness

Bedform generation under *monochromatic* waves propagating over a bed of uniform sand size has been extensively studied (e.g. Inman 1957, Dingler 1974, Carstens et al. 1969, Stefanick 1979, Nielsen 1981). Ripples start to form as the friction on the seabed increases from conditions just sufficient to initiate sediment motion (Madsen & Grant 1977). Two distinct regions of ripple growth and decay exist. In the first range (the equilibrium range) the ripple steepness, defined as the height-to-length ratio, approaches a maximum, and the ripple length is proportional to the near-bottom wave orbital excursion amplitude. With an increase in friction beyond the equilibrium range, a decrease in ripple steepness occurs that is associated with a decrease in ripple height and a simultaneous decorrelation between

excursion amplitude and ripple length. This nonequilibrium region is called the breakoff region (Inman 1957). Ripples are obliterated by the flow for sufficiently large values of the boundary shear stress so that a flat bed condition occurs. The transition in ripple geometry is accomplished by an increase in near-bed sediment transport.

A relationship between ripple geometry, sediment characteristics, and the wave boundary shear stress has been empirically derived by Stefanick (1979). Empirical relationships relating potential-flow characteristics of waves to ripple geometry have been suggested by Nielsen (1981), while Miller & Komar (1980a) have related the limiting ripple geometries (i.e. initial ripple generation, and disappearance) to both boundary shear stress and sediment characteristics.

Grant & Madsen (1982) used a semiempirical approach to derive an expression for the roughness of movable beds under waves. The roughness depends on both bed geometry and near-bed transport. For quartz sand, their expression is $z_0 = 16.8d\psi_{cr}[(\psi'/\psi_{cr})^{1/2} - 0.7]^2 + 0.93(\eta/\lambda)\eta$, where ψ' is the Shields parameter based on grain-size, d, roughness, and the subscript cr denotes the value at initial motion (see Madsen & Grant 1977). The first term, expressing the roughness contribution from the near-bed transport, is comparable to the steady-flow equation of Smith & McLean (1977a). The contribution from the form drag over the ripples, given by the second term, follows a "k, δ" roughness scaling, and the expressions for the ripple geometry may be evaluated from empirical relationships (Stefanick 1979). A similar, totally empirical expression for the ripple form-drag roughness was derived by Swart (1977) using different data; this resulted in a coefficient of 0.83 as compared with 0.93 above. It should be emphasized that these relationships are limited to fine sands or coarser.

Biological Effects on Bottom Roughness

Roughness due to bedforms and near-bed transport is directly related to the flow dynamics through the instability mechanism that generates the sediment transport and bedforms and through the feedback of the roughness on the flow dynamics. These processes are important for relatively strong flows, since sediment motion must be initiated, and they are generally limited to sandy sediments. Many continental-shelf regions [e.g. the Coastal Ocean Dynamics Experiment (CODE) site, Mud Patch on the east coast of the United States, the Washington Shelf] contain large regions of silty sands or mud in which flow-induced bedforms are not generally observed, except possibly in very strong flows when a large enough fraction of coarser sediment is left on the bed for bedforms to develop. Over muddy bottoms during typical nonstorm flows, observations (e.g. Chriss & Caldwell 1982, Cacchione et al. 1983, Butman 1985) indicate

that the microtopography of the seabed is controlled primarily by biological mechanisms. This biological microtopography is highly variable depending on the organisms present, their abundances, the nature of their activity, and the sediment type. It is expected that biological activity will vary seasonally as a result of such things as physical-oceanographic processes (e.g. upwelling) and reproduction cycles.

Biological mechanisms can influence the bottom roughness through at least three distinct mechanisms (Rhoads & Boyer 1982, Nowell et al. 1981). (*a*) They can make the bed bumpy from activities such as burrowing, tube building, and fecal pellet production. (*b*) The actual animals themselves can act as roughness elements. (*c*) They can modify the sediment characteristics and thus the sediment transport through adhesion (Nowell et al. 1981, Grant et al. 1982) and vertical mixing of sediment particles.

The importance of biologically induced roughness to the boundary-layer flow and to the general shelf circulation should not be minimized. For muddy bottoms with no bioturbation the flow away from the bed would be expected to be hydrodynamically smooth [$z_0 = O(10^{-3}$ cm)], with a corresponding drag coefficient (referenced to one meter) $C_{D100} \leq 1.5 \times 10^{-3}$. With bioturbation, observations indicate the flow is hydrodynamically rough [$z_0 = O(0.1$ cm); e.g. Soulsby 1983, Grant et al. 1984], with a corresponding drag coefficient $C_{D100} = 3 \times 10^{-3}$. Thus, the mean friction, important to the shelf circulation, may be increased by more than a factor of 2 as a result of biological activity.

Despite its potential importance, little work of a general nature has been done on relating biologically created microtopography to the roughness length. In fact, very few continental-shelf boundary-layer studies have even cited biological roughness as being important.

Roughness Estimates for the Field

In spite of progress in several critical areas, much remains to be done on the roughness problem. On wind-driven continental shelves the situation of general interest is the combined presence of waves and currents. The roughness relationships discussed above are based on data for pure currents or pure waves. Wave-formed ripples are typically found on sandy bottoms under wave-dominated conditions (Butman 1985, Cacchione et al. 1983, 1984, Miller & Komar 1980b, W. D. Grant & D. A. Cacchione, in preparation). For mud bottoms, bioturbation dominates in nonstorm cases. It appears that the roughness estimates calculated from distributed-roughness models work reasonably well, provided the ripple roughness is sufficiently small relative to the wave-boundary-layer thickness for the microtopography to be considered as roughness elements. The thickness of the planetary and wave boundary layers are orders of magnitude different,

so there is clearly the potential for the existence of a wide range of roughness-length scales. The largest of these roughness scales cannot satisfy the required bounds for the existence of a logarithmic velocity profile in the wave boundary layer. For the combined-flow case, additional topographic roughness scales much larger than δ_{cw} can influence the roughness of the outer boundary layer while introducing local modifications of the wave velocity.

Even for wave-dominated ripples, the situation can be complicated. In coarser sediments, ripples may form only under storm conditions and therefore be preserved in a state that is not in equilibrium with nonstorm conditions that are too weak to move the sediment (Cacchione et al. 1984). These bedforms then exceed the wave-boundary-layer thickness under nonstorm conditions and do not act as roughness elements to the waves. Waves approaching from different directions either simultaneously or at different times can form sets of ripples at oblique angles to the flow for which the roughness is not known. For shallow water with orbital velocities due to several different wave frequencies reaching the bottom, little is known about the resulting ripple field. Currents can form bed features with roughness scales large compared with the wave-boundary-layer thickness, and the waves feel these as topographic features. However, small wave-formed ripples may develop on or around such bed features. When wave-current interaction is considered, these situations require careful analysis and are considerably more complicated than the problem treated by Smith & McLean (1977a).

For biologically dominated roughnesses, little is known about the behavior of such features and the animals that make them when subject to flow conditions with large boundary shear stresses relative to the critical motion value. The recovery time required for the biological reworking to dominate the bed features after mechanical reworking is also unknown, as are the scales of variability and seasonal dependency of biologically created roughness.

OTHER PROCESSES AFFECTING THE BOUNDARY LAYER

The effects of roughness and wave-current interaction are accepted as being important to the boundary-layer dynamics on wind-driven shelves. At this point, data sets, several of high quality, are available on aspects of these processes, and there is reasonable correspondence between theoretical ideas and observation. All of these detailed data are for the near-bottom flow in the region 5 m $> z >$ 30 cm, and therefore they leave out important regions of the boundary layer and cover only intermediate scales. Other

processes are known or have been suggested as being important to shelf boundary-layer dynamics, but in many of these cases either the dynamic mechanisms are not yet quantitatively well formulated or insufficient observational evidence is available to demonstrate their relative importance. In the following we summarize some of these concepts that will be important to future advances in continental-shelf boundary-layer research.

Stratification

The water column on the continental shelf generally exhibits vertical gradients in density associated with gradients in temperature, salinity, and (in special cases) suspended sediment. As a rule, less-dense water overlies denser water, and the resulting stratification is stable. On the shelf a region of well-mixed fluid is almost always found (Caldwell 1978, Grant et al. 1984) for the first few meters above the bottom, except in the case where extensive suspended sediment occurs.

The effect of stable stratification on the mean and turbulent structure of boundary-shear flows is well known. Vertical mixing is damped, since shear production of turbulence is partially reduced by work against buoyancy forces. The net result is that diffusion of momentum and mass within the boundary layer is reduced. The boundary layer is reduced in thickness from the neutral case, and for the same external driving velocity, the boundary shear stress is decreased and the veering angle is increased.

The effect of stratification is formally expressed by the dimensionless ratio of energy absorbed by buoyancy forces to production by mean shear (called the flux Richardson number Ri_f). This number involves fluctuating quantities that are difficult to measure in practice, so the gradient Richardson number $\mathrm{Ri}_g = -(g/\rho)\partial\rho/\partial z/(\partial u/\partial z)^2$ is generally used in applications. Miles (1961) showed that inviscid stratified flow was stable for $\mathrm{Ri}_g > 0.25$ everywhere in the flow. In fact, this value for Ri_g is only an estimate, and stability is a continuous rather than abrupt process.

No complete data set on stably stratified continental-shelf bottom boundary layers has been published to date. Published data sets for continental shelves are limited to near-bottom measurements in the inertial layer, where the flow is neutral (Grant et al. 1984, Cacchione & Drake 1982, D. A. Cacchione et al., in preparation) or to outer-layer measurements without benefit of direct stress or inertial-layer measurements (e.g. Weatherly & Van Leer 1977, Dickey & Van Leer 1984). Thus, our present quantitative knowledge of stratified marine bottom boundary layers comes from models. Various models treating stably stratified, rotating boundary layers have been developed (Businger & Arya 1974, Weatherly & Martin 1978, Mellor & Yamada 1974, Long 1981) as extensions of planetary boundary-layer models to the marine boundary-layer case, with little or no

unique developments specific to the marine case and little direct testing, due to the lack of data, of the "universal" coefficient contained in these models. These models do provide, however, a picture of the qualitative features of the boundary layer, and it appears reasonable to consider the bottom boundary layer as generally stably stratified in the outer region owing to temperature and salinity. Moreover, advection often appears to be able to maintain the stratification in spite of strong mixing.

SUSPENDED SEDIMENT STRATIFICATION Smith & McLean (1977a,b) developed a near-bottom quasi-steady flow model for a bottom boundary layer subject to suspended-sediment-induced stratification. Adams & Weatherly (1981) extended the work of Smith & McLean (1977a,b) to a planetary boundary layer. These models couple the conservation of mass and momentum through the effect of the mass field on the vertical mixing of momentum. Near the boundary, an alternative to the Richardson number is the nondimensional stability parameter z/L. Here $L(=-\rho u_*^3/g\langle\rho' w'\rangle)$ is the Monin-Obukov length, where ρ' and w' are the fluctuating density and turbulent vertical velocity, respectively. The parameter z/L expresses the ratio of turbulent kinetic energy dissipated by buoyancy forces to that produced by mean shear in the vicinity of the boundary where the production is equal to $u_*^3/\kappa z$. The introduction of the stability parameter allows a useful analogue between log-linear atmospheric models of stably stratified shear flows in the surface layer and suspended-sediment stratification in the ocean. Thus, the effect of the suspended-sediment-induced stratification on the velocity profile in the overlap layer is similar to the results from atmospheric models for stratification due to surface heating. Stratification is expressed in terms of the stability parameter and results in the velocity profile

$$u = \frac{u_*}{\kappa}\left(\ln\frac{z}{z_0} + \int_{z_0}^{z} \beta\frac{dz}{L}\right), \tag{28}$$

where β is a coefficient equal to 4.9 (Businger & Arya 1974). For the suspended-sediment case the stability parameter can be expressed as $z/L = (\kappa z/u_*^3)\sum_n g(s_n-1)w_{fn}C_n$, where w_f is the fall velocity, C is the mean concentration, and the subscript n denotes the nth size class. Equation (28) illustrates that the stratification is not governed by total concentration but by the product of the concentration and the fall velocity. Moreover, the stratification depends on the integral over all levels below. Thus, a large concentration by itself has little relevance to the stratification problem. Fine sediments that are uniformly mixed upward can be present in large concentrations but have no significant gradient and have little stratification potential, whereas coarse sediments may have strong gradients but remain

close to the boundary and therefore also have little effect on stratification. Equation (28) and the expression for z/L above also point out two major problems with suspended-sediment calculations: To calculate the integral, both the concentration near the bed and the fall velocity for each size class must be known. Although several models exist for the reference concentration (e.g. Smith & McLean 1977a,b, Grant & Glenn 1983), this concentration is presently difficult to estimate. The fall velocity for fine sediment in the field is equally difficult to estimate because of flocculation.

STRATIFICATION IN WAVE AND CURRENT FLOWS In the case of combined waves and currents, the ability of the flow to stratify and the effects of the stratification on the flow are strongly tied to the waves. For temperature and salinity stratification in the outer-flow region, the mixing is affected by the waves through the enhanced turbulence production by mean shear and Reynolds stress (represented by u_{*c}) at the boundary caused by wave-current interaction. For suspended-sediment stratification, the wave effects are extremely important. The large boundary shear stresses associated with the waves result in a large supply of sediment available to be mixed upward into the flow.

S. M. Glenn & W. D. Grant (in preparation; see also Grant & Glenn 1983, Glenn 1983) have treated the problem of self-stratification by suspended sediment in a stably stratified, rotating boundary layer subject to wave-current interaction by using a numerical model. Wiberg & Smith (1983) have described a similar model for fine sediment. S. M. Glenn & W. D. Grant (in preparation) find that stratification does not occur within the wave boundary layer for conditions expected on the shelf, since the concentration gradients are not large in this region and the stability parameter is small. In the region above the wave boundary layer, the vertical extent of the stratification due to suspended sediment is found to be self-limiting, since the neutral decay rate of the concentration with height in the Ekman layer is multiplied by a further exponential decay factor dependent upon the stability parameter. Stratification of the outer layer of the boundary layer by temperature and salinity gradients helps to further limit the effects of suspended sediment to the lower part of the boundary layer. The net result is that temperature and salinity stratification tends to influence mainly the outer regions of the Ekman layer, while suspended-sediment-induced stratification tends to influence the lower part of the Ekman layer.

INTERNAL WAVES When stratification occurs on the shelf, internal waves can be generated in the frequency band between the Brunt-Väisälä frequency and the inertial frequency. These wave motions will have a boundary-layer scale $\kappa u_{*clw}/\omega_{lw}$, where the subscript Iw denotes internal

wave. This scale can be comparable to the full Ekman-layer depth or can be *relatively* smaller. For higher frequencies and linear internal waves, these boundary layers can be treated as oscillatory boundary layers. Many internal-wave events on the shelf are intermittent and the waves nonlinear (Sanford 1984), and time-dependent boundary-layer models are more appropriate. For low-frequency waves, where δ_{Iw} is greater than the mixed-layer depth, rotating, stratified time-dependent boundary-layer dynamics are appropriate.

Internal waves can have two types of effects on the planetary boundary layer (Grant 1982). First, they can kinematically distort the velocity profile in the overlap layer for situations where small time averages are taken relative to the internal-wave period. This can result in erroneous values of z_0 and u_*, depending on the time period the average is taken over, as well as in curvature of the profiles. Secondly, there is the potential for wave-current interaction or surface-wave–internal-wave–current interaction. Sanford (1984) has treated this case and demonstrated that quite complicated velocity profiles and stress profiles can be produced. Grant et al. (1984) have noted significant distortion of time average velocity profiles within the inertial layer during times of pronounced internal-wave activity.

Other Qualitative Effects

TOPOGRAPHY, ACCELERATION, AND DECELERATION The descriptions of the boundary layer given above assumed that the topography of the seabed could be considered as roughness elements such that the associated hydrodynamic length scale z_0 was much smaller than δ. Clearly, many cases of practical interest involve topographic features too big to be treated as roughness. Flows over such features involve accelerated and decelerated regions over the topography. The equations of motion must be modified by the addition of convective acceleration terms $u_i(\partial u_j/\partial x_i)$. The model of Smith & McLean (1977a) is a convenient method to treat the zero-order flow over such features for weak acceleration. This model could be extended to include wave-current interaction, although this has not yet been done. Decelerations and accelerations can modify the mean velocity profile near the boundary. Generally, accelerated flows are treated separately, since their effects can involve relaminarization of the flow. The effects of adverse pressure gradients (see Kader & Yaglom 1978, Yaglom 1979) can be estimated using similarity theory in much the same way that stratified flows are treated. An additional length scale $\delta_p = \rho u_*^2/|dp/dx|$ is introduced. The presence of an additional scale imposed by the pressure gradient requires that this scale must now be considered when defining the matching in the overlap layer, and thus log profiles are not guaranteed. The outer flow or the wall flow can be modified in the same way that stratification modified the flow.

SURFACE MIXED-LAYER AND BOTTOM BOUNDARY-LAYER INTERACTIONS For typical nonstorm conditions in the mid- and outer-shelf regions, the surface mixed layer and bottom layers are well separated by a geostrophic core region. In storms the surface mixed layer and the bottom boundary layer can merge over much of the shelf. In addition to the complicated entrainment mechanisms causing growth of the surface mixed layer (e.g. Niiler 1975), wave breaking in the surface layer can mix momentum downward. In the bottom boundary layer, large storm waves can greatly enhance the mean friction that is related to the production of turbulence for mixing. Other mixing processes such as Langmuir circulations (Leibovich 1983) are of equal or more importance to mixing and are also believed to be related to wave behavior. Thus, important mechanisms for growth of each layer are related to surface-wave behavior.

Again, the quantitative description of this problem is data limited. Presently, the role of wave breaking in the dynamics of surface mixed layers is also poorly understood, but sufficient evidence exists to believe that it may be an important mechanism during large wave events (e.g. see Thorpe 1984, W. K. Melville, personal communication).

MEASUREMENTS

Field measurements of velocity profiles and stress estimates in combined wave and current flows have been reported by Cacchione & Drake (1982), D. A. Cacchione et al. (in preparation), Grant et al. (1984), and W. D. Grant & D. A. Cacchione (in preparation).

Cacchione & Drake (1982) measured velocity profiles in the lower meter of the water column, in a combined wave and current flow over a mud bottom in Norton Sound. Their measurements show the mean velocity profiles to be logarithmic and with the estimated (using the profile technique) values of u_* and z_0 much larger than expected for the corresponding observed bottom roughness. Comparisons with GM and J. D. Smith's theories for u_* were quite good, but the theories overpredicted the roughness. Cacchione & Drake (1982) attributed this difference to potential stratification by suspended sediment. Wiberg & Smith (1983) reanalyzed the data, employing a zero shift in the velocity profile to account for settlement of the tripod into the bottom and possible flow blockage by the tripod, and found good agreement with theory; their results showed that stratification was unlikely owing to the uniform distribution of suspended sediment.

Grant et al. (1984) carried out measurements as part of CODE on the Northern California Shelf. They measured velocity profiles within 2 m of the bottom using two or three tripods deployed simultaneously over a flat bottom covered with small (<1 cm) biologically generated roughness.

Stress was estimated using both the velocity-profile and the inertial-dissipation techniques. Their results showed good agreement with predictions of wave-current theories for the mean stress and apparent roughness during periods of large relative wave velocities. When the relative wave velocities were small compared with the velocity of the current, the estimated roughness and shear velocity agreed well with the bottom roughness and shear velocity corresponding to the observed microtopography. Bottom stress estimates from the velocity-profile techniques showed good agreement with estimates made from the inertial-dissipation technique. Stress profiles estimated using the dissipation technique showed reasonable correspondence with the asymptotic relationship for the planetary boundary layer (see also Grant & Williams 1985). W. D. Grant & E. A. Terray (in preparation) estimate stress for the same data set using the eddy-correlation technique; they find good agreement between the three estimation techniques after correcting for erroneous wave contributions to the stress caused by tilt of the reference coordinate system. W. D. Grant & D. A. Cacchione (in preparation), also as part of CODE, analyzed velocity-profile measurements made over a sand bottom covered with wave-formed ripples and found good agreement with the wave-current interaction models for flow over wave-generated bedforms.

D. A. Cacchione et al. (in preparation) analyzed velocity-profile measurements made in 70-m water depth during a winter storm off the Russian River Shelf and found reasonable correspondence between the mean shear stress and apparent roughness values estimated from the data and the values predicted from the Grant & Madsen (1979, 1982) models. Mean shear velocities exceeded 5 cm s^{-1}, and the apparent roughness was over 6 cm. No stratification appears to have occurred in spite of peak suspended-sediment concentrations larger than 5×10^{-5}, since the primarily silty sediment was vertically well mixed. To maintain good correspondence between model and measurements, movable bed effects had to be accounted for in changes in the bottom roughness.

All of the data sets above were taken outside the wave boundary layer ($z > \delta_{cw}$) over relatively uniform bottoms, with roughness elements such that $z_0 \ll \delta_{cw}$. Thus, they represent good tests of the simplest versions of the wave-current boundary layer and bottom-roughness model (i.e. no topographic effects need be accounted for). The analyses cited indicate good correspondence with logarithmic velocity profiles. This agreement is somewhat deceiving, however, since most of the tripods depend on the profile technique to make stress estimates, and thus the analyses usually concentrate on data exhibiting this feature. Grant et al. (1984) found that the measured profiles during a 15-hr period analyzed at the CODE site could be considered strongly logarithmic (regression coefficient $R > 0.997$)

only 30% of the time as a result of distortion of the flow by internal waves. In spite of large values of the regression coefficient ($R > 0.96$) the rest of the time, the profiles were argued to deviate from the log form, and in fact the velocity profiles appear to be combinations of a log profile corresponding to the low-frequency flow with a superposed internal-wave boundary-layer velocity. This type of problem is typical of many shelf situations and is indicative of the complexity in measuring and interpreting velocity profiles.

Only Chriss & Caldwell (1982) have made field measurements of current speed below 20 cm from the bottom during combined wave and current flows. The authors find segmented velocity profiles (i.e. profiles with two different slopes) that they attribute solely to the effect of two different roughness scales associated with the presence of biologically generated bedforms on the muddy bottom at the site. They conclude that there are no wave effects on the mean velocity profile. However, their data set and analysis have several shortcomings: (*a*) The velocity measurements appear to be aliased by the waves as a result of the sampling scheme used in their profiling technique, and the wave motion cannot be resolved from their data; (*b*) no direct observations of the bottom or measurements of the bedform geometry were made at the site; and (*c*) their estimate of the wave boundary-layer thickness is based on the assumption of laminar flow. Regrettably then, their conclusions from this unique set of measurements are questionable, since they have no way to separate the effect of bedforms from wave-current interaction.

The lack of measurements in the wave boundary layer is a major shortcoming, since the mechanism of wave-current interaction depends on the behavior within this layer. A variety of relative wave and current conditions have been observed over the same bottom microtopography and show the expected decrease in roughness toward the physical bottom roughness as the currents become large relative to the wave. Also, for well-documented microtopography, the corresponding drag coefficients are much larger (by factors of 2 to 5) than predicted based on the topography alone. This is strong evidence of the mechanism of wave-current interaction, but by no means proof. It would appear that the detailed measurements required to test wave-current boundary-layer models must rely on laboratory experiments.

Laboratory studies of wave-current interaction over a rough bottom have been carried out by Bakker & van Doorn (1978) and Kemp & Simons (1982). Both of these studies show qualitative agreement (for runs with fully rough flows) with the enhanced roughness length and shear velocity predicted by the theories. For runs over a smooth bottom, the results of Kemp & Simons (1982) indicate no enhancement, as expected.

The problem with laboratory experiments is the necessity of using

extremely large roughness elements in order to achieve fully rough turbulent boundary-layer flows. In fact, both studies mentioned above employed a roughness that violates the requirement for the existence of an overlap layer ($z_0 \ll \delta_w$). Detailed comparison of theoretical predictions with these data is therefore of no merit unless a theory corresponding to the experimental conditions is developed.

MEASUREMENT PROBLEMS

The mean velocity profile is the end result of the dynamics present in the boundary layer, and it is often difficult to study the dynamics based on only this profile. Of more direct dynamical significance are the distribution of turbulent kinetic energy (TKE), wave kinetic energy (WKE), dissipation, and Reynolds stress. In addition, the value of the boundary shear stress and its relation to the roughness scale for the flow are of major importance to model testing. For the typical situation on wind-driven continental shelves, the direct measurement or estimation of these quantities from indirect measurements is greatly complicated by the presence of surface waves. We briefly review some of the major problems.

Kinetic Energy and Spectra

Figure 3 shows a typical horizontal velocity spectrum corresponding to velocities measured at 1 m above the bottom at a midshelf location on the continental shelf. The spectrum is dominated by the wave peak at $\sim$0.065 Hz. The peak in the TKE spectrum in wave-number space is expected to be in the vicinity of $2\pi/z$. Application of the Taylor hypothesis (Lumley 1965) to convert wave number to frequency demonstrates that the WKE peak sits on top of the region of peak TKE. This behavior is typical for bottom boundary layers on wind-driven shelves, and we have indicated in Figure 3 the range of wave frequencies expected on the shelf, relative to the TKE peak, for a 10 cm s^{-1} bottom flow. Typically the rms turbulent velocity fluctuation for the mean flow is O (10%) of the mean velocity, so that for equal wave and current velocities at 1 m, the WKE is $O(10^2)$ TKE.

The separation of WKE and TKE is a difficult problem. Linear-filtration techniques, which depend on an independent measure of the waves, such as pressure or surface elevation, appear to be prime candidates and have been tried by Thornton (1979), Lumley & Terray (1983), and W. D. Grant & E. A. Terray (in preparation). These techniques require calculation of the coherence between the total velocity and the independent wave measurement, assuming the wave and turbulence are uncorrelated. While it appears the latter assumption is justified on physical grounds, W. D. Grant & E. A. Terray (in preparation) find that the coherence function for real data is

extremely noisy as a result of stationarity requirements and results in poor separation. Nonlinear techniques have not been used and may ultimately be the answer. At present, estimates of WKE and TKE can be made using some wave theory to calculate the WKE from the independent measure of the waves and subtracting this from the total velocity variance to get an estimate of the TKE.

Near the bottom, vertical wave velocities are small and the energy spectrum is relatively uncontaminated by waves. W. D. Grant & E. A. Terray (in preparation) have found that for this case, estimates of quantities such as $\langle w'^2 \rangle / u_*^2$ agree well with classical expectations. This result indicates that the inertial region of the planetary boundary layer scales as expected.

Lumley & Terray (1983) have carefully investigated the application of

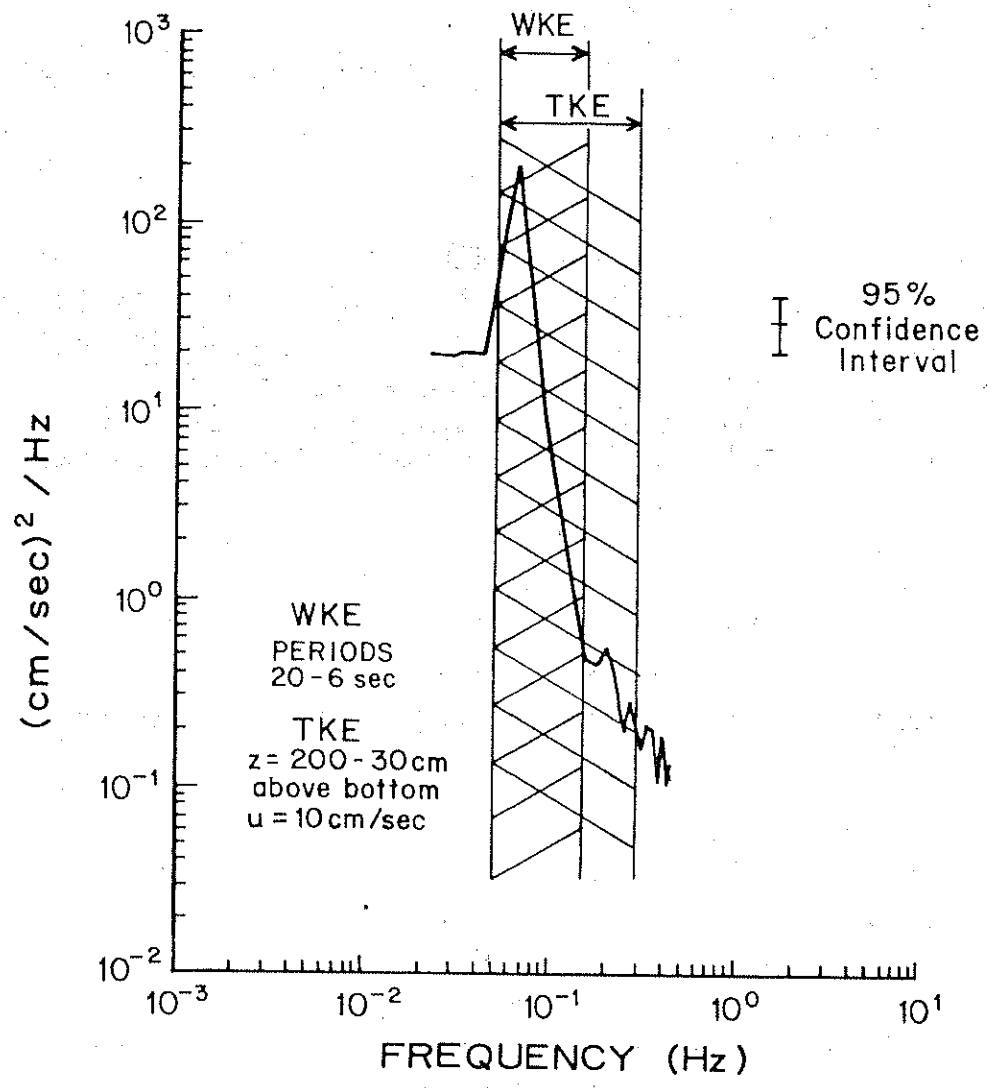

Figure 3 Spectrum of horizontal velocity measured 1 m above the ocean bottom. The overlaid frequency ranges correspond to kinetic energy for 6–20 s waves and peak turbulent kinetic energy for heights 30–200 cm above the bottom in a 10 cm s^{-1} flow.

Taylor's hypothesis to spectra measured in the presence of surface waves. Their study shows that the distortion of the inertial range of the spectrum occurs from advection of turbulent fluctuations by the wave orbital velocity and results in an apparent shift in the level of energy in the subrange on either side of the wave peak. This shift, if not properly accounted for, can result in large errors in making dissipation estimates from inertial-range spectra.

Reynolds-Stress Calculations

Reynolds stress can be calculated indirectly using the velocity-profile and inertial-dissipation techniques. The velocity-profile technique gives only the boundary shear stress and requires highly logarithmic velocity profiles. This technique has been used successfully on wind-driven shelves (Cacchione & Drake 1982, Grant et al. 1984).

The interpretation of velocity profiles as being logarithmic is a subjective undertaking. Typically, a straight line is fitted to a semilogarithmic plot of log z versus measured velocity using regression analysis. The primary measure of the logarithmic fit is the value of the regression coefficient R. The associated confidence bands on estimates of u_* and z_0 depend on this regression coefficient, on the number of measurement points, and on their spacing (Gross & Nowell 1983, Grant et al. 1984). The size of the acceptable errors on u_* and z_0, along with knowledge of the flow being measured and the instrument resolution, decides whether a profile is to be considered logarithmic. As an example, for four measurement points at 30, 50, 100, and 200 cm above the bottom, R-values of 0.997 and 0.950 correspond to 95% confidence bands of $\pm 25\%$ and $\pm 100\%$ on u_*, respectively. Figure 4 illustrates two velocity profiles measured at a midshelf location (Grant et al. 1984) several hours apart. In spite of the fact that both profiles appear highly logarithmic in the plots, only Figure 4*a* is considered logarithmic ($R = 0.9993$). The R-value in Figure 4*a* corresponds to a $\pm 11\%$ confidence band (at a 95% significance level) on u_*. The profile in Figure 4*b* ($R = 0.9866$) has been rejected because of an unacceptable $\pm 50\%$ confidence band on u_*. The departure of the profile in Figure 4*b* from logarithmic can be justified on physical grounds because of contamination by internal-wave effects that distort the profile (Sanford 1984). The interpretation of velocity profiles as being logarithmic, and thus of their being useful in making stress and roughness estimates, must be done with great care.

The inertial-dissipation technique suffers from the problem of contamination by waves, as well as from the requirement that assumptions be made on the TKE balance. In addition, the technique requires a sensor that can measure in the inertial subrange region of the spectrum. For near-bottom flows, where the vertical wave velocity is small, it has been successfully

applied to vertical density spectra by Grant et al. (1984). A general evaluation of this technique is given by Lumley & Terray (1983).

Direct estimates of Reynolds stress can be made using the eddy-correlation technique. Applications of this technique to the upper-ocean mixed layer have resulted in large contributions to the total momentum flux at wave frequencies (e.g. Cavaleri & Zecchetto 1985). No reasonable physical mechanism has been offered for these fluxes at the wave frequencies, since, for irrotational waves, the time-averaged product of the horizontal and vertical velocities is zero. W. D. Grant & E. A. Terray (in preparation) have shown that the explanation for these fluxes appears to be in errors associated with rotations of the measurement coordinate system from the true coordinate system that are identical to the usual tilt error cited in Reynolds-stress measurements. The true $\langle uw \rangle$ product is related to the tilted $\langle u_i w_i \rangle$ in the system by $\langle u_i w_i \rangle = \langle uw \rangle (1 + [\langle w^2 \rangle - \langle u^2 \rangle]\theta / \langle uw \rangle)$,

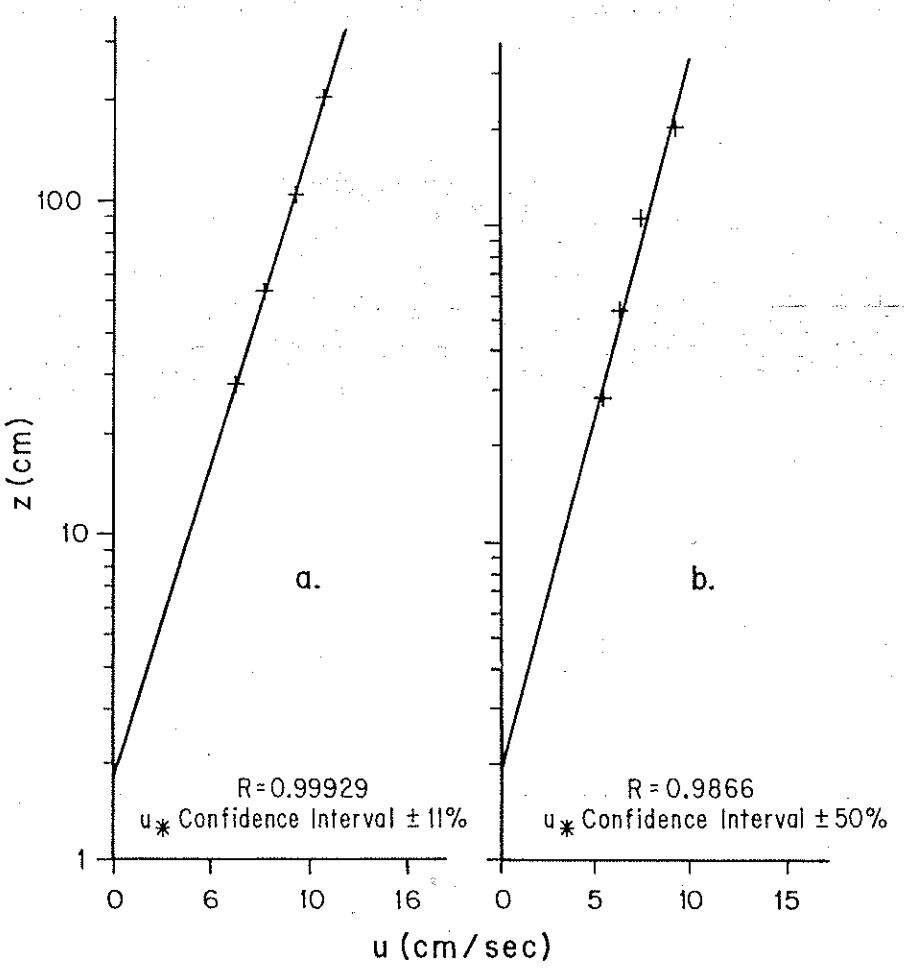

Figure 4 Measured mean velocity (plus) compared with logarithmic profile (solid line) for $z > \delta_{cw}$. Regression coefficients are indicated with corresponding 95% confidence interval on u_*. (*a*) True logarithmic profile; (*b*) distorted profile caused by the presence of internal waves.

where the tilt angle θ is assumed small. Thus, in the bottom boundary layer the vertical velocity variance for the wave is much less than the horizontal velocity variance, and thus the error is proportional to $\langle u_w \rangle^2 / \langle uw \rangle \theta$. Even for a small tilt of 1–2° this error, which occurs at the wave frequency, is large and can swamp the true turbulent Reynolds-stress contribution; higher up in the boundary layer, where w_w can be significant, this error should decrease. However, for a spectrum of waves, proper averaging is critical and potential errors again exist.

The Wave Boundary Layer and Roughness

The scale of the wave boundary layer is small compared with that of conventional sensors and places strong constraints on the instrumentation used to investigate it. Moreover, as with all boundary layers, the definition of its upper limit and the displacement height make its exact resolution difficult. Thus, making velocity measurements of either the mean flow or turbulence in this region is extremely difficult in the field.

Resolution of the small-scale roughness is an important part of the wave boundary-layer measurement problem. The roughness scale seen by the flow within the wave boundary layer is related to the total force acting over all the roughness elements rather than to the details of the flow around an individual roughness element, so that a spatial average over many roughness elements is needed. For relatively nonuniform roughness elements, accurate determination of this roughness scale from measurements of microtopography depends on the ability to estimate the displacement thickness, which depends strongly on the nonuniformity and types of roughness elements.

The wave-current interaction model predicts that the apparent mean shear velocity within the wave boundary layer is given by $u_{*c}(u_{*c}/u_{*cw})$, and thus use of the velocity-profile technique to estimate stress requires an independent estimate of u_{*c} from above the wave boundary layer or of u_{*cw} within the layer.

Sediment-transport effects were seen to play an important role in the roughness scales. Sediment-transport prediction requires accurate estimates of the skin friction. For distributed roughness elements, this means that enough individual point measurements must be made to make a proper spatial average to relate back to the average skin friction. To resolve the roughness associated with the near-bed transport requires near-bed estimates of the transport based on some direct or remote measurement technique.

As the boundary-layer scale increases, the roughness length scale also increases. Since the total roughness scale is an average of the details of

individual roughness elements, the horizontal scales associated with the average increase as one moves away from the boundary. This has a tendency to smooth out variability in the roughness, due to physical and biological mechanisms such as sediment-size changes or mixtures and variability in benthic biota, seen by the large-scale flow. However, it also makes it difficult to compare point estimates of stress, and careful estimates of resolution and expected variability must be made to plan experiments properly.

The Outer Boundary Layer

The location of the top of the boundary layer is dependent upon the definition used (for example, whether a percentage of the external velocity or of the boundary shear stress is used). In the usual field situation involving stratification, this location is difficult to measure precisely. For the case where both surface and bottom layer mix, no rational definition of the end of one layer and the beginning of another appears possible. Thus, it is extremely important to have continuous vertical profiles of the important dynamical quantities identified here to compare with predictions from various models that serve the function of organizing the important physics.

FUTURE WORK AND PERSPECTIVE

Improvements in our understanding of wind-driven continental-shelf bottom boundary-layer flows require a substantial increase in the existing data base and the associated theoretical developments. Classical boundary-layer theory forms an important base, but the complications introduced for the shelf flow field require careful consideration of the multitude of processes present and their interaction. Proper inclusion of the processes dictates a cross-scientific approach. Surface waves can no longer be considered simply as high-frequency noise in the system, nor can the presence of sediment transport and bioturbation be considered inconvenient problems facing only geologists and biologists. Because of the nonlinearities in the system, time averages at all time scales, whether surface waves, internal waves, or tides, need to be considered properly. The simple boundary-layer models for monochromatic waves need to be extended to consider a spectral representation of the waves.

The careful use of theory to design experiments is essential to acquiring high-quality and interpretable data sets. It is no longer acceptable to explain large roughnesses by "unobserved upstream bumps." Experiments to test models must correspond to the assumptions in the model. Measurement errors must be carefully evaluated. The total dependence on

the existence of or the ability to measure logarithmic velocity profiles to estimate stress and roughness has nearly as many problems as other estimation techniques. Redundant measures are called for.

Many of the areas where work is needed are identified in the text. Three notable topics where little discussion of measurements was given are turbulence, the immediate vicinity of the bottom, and the outer boundary layer. Very few data exist on turbulence, and near-bed and outer boundary-layer measurements have not been taken simultaneously with inertial-layer measurements. This is surprising, since all boundary-layer model and data comparisons depend on such full data sets.

Near-bed measurements are most likely best carried out in the controllable laboratory environment, where a sufficient number of points can be measured to get proper spatial resolution, where proper instrument mounting and control can be achieved, and where accurate measurements or control of microtopography and sediment transport is possible. These results must then be parameterized to relate back to easily measured quantities in the field. The outer-layer measurements require velocity, temperature, and salinity data of sufficient accuracy to evaluate model closures. These measurements are likely to be influenced by large-scale structures, which affect mixing and about which little is known.

Although these problems are challenging, they are not insurmountable, and in fact their identification is possible only because our understanding of bottom boundary layers on wind-driven shelves has experienced significant advancements in recent years.

Acknowledgments

We wish to thank the graduate students at MIT and in the WHOI/MIT Joint Program in Oceanographic Engineering who have contributed greatly to the work summarized here. This review has benefited from valuable discussions with Professors J. D. Smith, A. R. M. Nowell, and W. K. Melville and Drs. R. C. Beardsley, D. A. Cacchione and K. H. Brink. We thank Mrs. Gretchen McManamin, who typed the manuscript, and Mrs. Betsey Hirschel, who did the graphics. The first author expresses his gratitude to the National Science Foundation, Physical Oceanography Program, for continued support for continental-shelf boundary-layer research and for support while writing this review under Grant OCE-8403249. Additional support also came from NOAA Sea Grant NA84AA-D-00033 and Office of Naval Research Grant N000-14-C-85-0001. The second author expresses his gratitude for the continued support from the NOAA Sea Grant Program at MIT. This article is Woods Hole Oceanographic Institution Contribution Number 5952.

Literature Cited

Abramowitz, M., Stegun, I. A., eds. 1972. *Handbook of Mathematical Functions, Natl. Bur. Stand. Appl. Math. Ser. No. 55.* Washington, DC: US Govt. Print. Off. 1046 pp.

Adams, C. E., Weatherly, G. L. 1981. Some effects of suspended sediment stratification on an oceanic bottom boundary layer. *J. Geophys. Res.* 86(C5):4161–72

Allen, J. K. L. 1968. *Current Ripples.* Amsterdam: North-Holland. 149 pp.

Allen, J. S. 1980. Models of wind-driven currents on the continental shelf. *Ann. Rev. Fluid Mech.* 12:389–433

Bakker, W. T., van Doorn, Th. 1978. Near-bottom velocities in waves with a current. *Proc. Coastal Eng. Conf., 16th,* pp. 1394–1413

Blackadar, A. K., Tennekes, H. 1968. Asymptotic similarity in neutral barotropic planetary boundary layers. *J. Atmos. Sci.* 25:1015–20

Bowden, K. F. 1962. Turbulence. In *The Sea,* Vol. 1, ed. M. N. Hill, pp. 802–25. New York: Wiley-Interscience

Bowden, K. F. 1978. Physical problems of the benthic boundary layer. *Geophys. Surv.* 3:255–96

Brevik, I. 1981. Oscillatory rough turbulent boundary layers. *J. Waterway, Port, Coastal Ocean Div., ASCE* 107(WW3): 175–88

Businger, J. A. 1974. Aerodynamics of vegetated surfaces. In *Heat and Mass Transfer in the Biosphere,* Vol. 1. *Transfer Processes in the Plant Environment,* pp. 139–65. Washington, DC: Scripta

Businger, J. A., Arya, S. P. S. 1974. Height of the mixed layer in the stably stratified planetary boundary layer. *Adv. Geophys.* 18A:73–92

Butman, B. 1985. Physical processes causing surficial sediment movement in Georges Bank. In *Georges Bank Atlas.* Cambridge, Mass: MIT Press. In press

Cacchione, D. A., Drake, D. E. 1982. Measurements of storm-generated bottom stresses on the continental shelf. *J. Geophys. Res.* 87(C3):1952–61

Cacchione, D. A., Drake, D. E., Grant, W. D., Williams, A. J. III. 1983. Variability of seafloor roughness within the Coastal Ocean Dynamics Experiment (CODE) region. *WHOI Tech. Rep. 83-25,* Woods Hole Oceanogr. Inst., Woods Hole, Mass. 44 pp.

Cacchione, D. A., Drake, D. E., Grant, W. D., Tate, G. B. 1984. Rippled scour depressions on the inner continental shelf off central California. *J. Sediment. Petrol.* 54(4):1280–91

Caldwell, D. R. 1978. Variability in the bottom mixed layer on the Oregon Shelf. *Deep-Sea Res.* 25:1235–43

Carstens, M. R., Nielson, R. M., Altinbilek, H. D. 1969. Bed forms generated in the laboratory under oscillatory flow: Analytical and experimental study. *Tech. Memo. 28,* US Army Corps Eng., Coastal Eng. Res. Cent.

Cavaleri, L., Zecchetto, S. 1985. Reynolds stress under wind waves. In *The Ocean Surface: Wave Breaking, Turbulent Mixing, and Radio Probing,* ed. Y. Toba, H. Mitsuyasu, p. 586. Dordrecht: Reidel. In press

Chriss, T. M., Caldwell, D. R. 1982. Evidence of the influence of form drag on bottom boundary layer flow. *J. Geophys. Res.* 87(C6):4148–54

Clarke, A. J., Brink, K. H. 1985. The response of stratified, frictional flow of shelf and slope waters to fluctuating large scale low frequency wind forcing. *J. Phys. Oceanogr.* 15(4):439–53

Clauser, F. H. 1956. The turbulent boundary Layer. *Adv. Appl. Mech.* 4:1–51

Coleman, N. L. 1981. Velocity profiles with suspended sediment. *J. Hydraul. Res.* 19(3):211–29

Coleman, N. L. 1984. Discussion: Velocity profiles with suspended sediment. *J. Hydraul. Res.* 22(4):263–89

Dickey, T. D., Van Leer, J. C. 1984. Observations and simulation of a bottom Ekman layer on a continental shelf. *J. Geophys. Res.* 89(C2):1983–88

Dingler, J. R. 1974. *Wave-formed ripple in nearshore sands.* PhD thesis. Scripps Inst. Oceanogr., La Jolla, Calif. 136 pp.

Dyer, K. R. 1980. Velocity profiles over a rippled bed and the threshold of movement of sand. *Estuarine Coastal Mar. Sci.* 10:181–99

Glenn, S. M. 1983. *A continental shelf bottom boundary layer model: The effects of waves, currents, and a moveable bed.* ScD thesis. Mass. Inst. Technol., Cambridge. 237 pp.

Grant, W. D. 1977. *Bottom friction under waves in the presence of a weak current: Its relationship to coastal sediment transport.* ScD thesis. Mass. Inst. Technol., Cambridge. 275 pp.

Grant, W. D. 1982. The influence of internal waves on near-bottom velocity profiles measured on the continental shelf: Stress and roughness estimates. *EOS, Trans. Am. Geophys. Union* 63:45 (Abstr.)

Grant, W.D, Glenn, S. M. 1983. A continental shelf bottom boundary layer model. Vol. I. Theoretical development. *Tech. Rep. to the Am. Gas Assoc.* 167 pp.

Grant, W. D., Madsen, O. S. 1979. Combined wave and current interaction with a rough bottom. *J. Geophys. Res.* 84(C4): 1797–1808

Grant, W. D., Madsen, O. S. 1982. Moveable bed roughness in unsteady oscillatory flow. *J. Geophys. Res.* 87(C1): 469–81

Grant, W. D., Williams, A. J. III. 1985. Reply to Huntley: Discussion (Bottom stress estimates and their prediction on the northern California continental shelf during CODE-1: The importance of wave-current interaction). *J. Phys. Oceanogr.* 15(9): 1219–28

Grant, W. D., Boyer, L., Sanford, L. P. 1982. The effects of bioturbation on the initiation of motion of intertidal sands. *J. Mar. Res.* 40: 659–77

Grant, W. D., Williams, A. J. 3rd, Glenn, S. M. 1984. Bottom stress estimates and their prediction on the northern California continental shelf during CODE-1: The importance of wave-current interaction. *J. Phys. Oceanogr.* 14(3): 506–27

Gross, T. F., Nowell, A. R. M. 1983. Mean flow and turbulence scaling in a tidal boundary layer. *Cont. Shelf Res.* 2: 109–26

Hannan, C. A. 1984. Planktonic larvae may act like passive particles in turbulent near-bottom flows. *Limnol. Oceanogr.* 29: 1108–16

Huffman, G. D., Bradshaw, P. 1972. A note on von Karman's constant in low Reynolds number turbulent flow. *J. Fluid Mech.* 53: 45–60

Inman, D. L. 1957. Wave generated ripples in nearshore sands. *Tech. Memo. 100,* US Army Corps Eng., Beach Erosion Board. 41 pp.

Jackson, P. S. 1981. On the displacement height in the logarithmic velocity profile. *J. Fluid Mech.* 111: 15–25

Jonsson, I. G. 1966. Wave boundary layers and friction factors. *Proc. Coastal Eng. Conf., 10th,* pp. 127–48

Jonsson, I. G. 1980. A new approach to oscillatory rough turbulent boundary layers. *Ocean Eng.* 7: 109–52

Jonsson, I. G., Carlsen, N. A. 1976. Experimental and theoretical investigations in an oscillatory turbulent boundary layer. *J. Hydraul. Res.* 14(1): 45–60

Kader, B. A., Yaglom, A. M. 1978. Similarity treatment of moving-equilibrium turbulent boundary layers in adverse pressure gradients. *J. Fluid Mech.* 89: 305–42

Kajiura, K. 1964. On the bottom friction in an oscillatory current. *Bull. Earthquake Res. Inst., Univ. Tokyo* 42: 147–74

Kajiura, K. 1968. A model of bottom boundary layer in water waves. *Bull. Earthquake Res. Inst., Univ. Tokyo* 46: 75–123

Kamphuis, J. W. 1975. Friction factor under oscillatory waves. *J. Waterways, Harbors Coastal Eng. Div., ASCE* 101(WW2): 135–44

Kemp, P. H., Simons, R. R. 1982. The interaction between waves and a turbulent current: Waves propagating with the current. *J. Fluid Mech.* 116: 227–50

Lavelle, J. W., Mofjeld, H. O. 1983. Effects of time-varying viscosity on oscillatory turbulent channel flow. *J. Geophys. Res.* 88(C12): 7607–16

Leibovich, S. 1983. The form and dynamics of Langmuir circulations. *Ann. Rev. Fluid Mech.* 15: 391–427

Long, C. E. 1981. A simple model for time-dependent stably stratified turbulent boundary layers. *Spec. Rep. No. 95,* Dep. Oceanogr., Univ. Wash., Seattle. 170 pp.

Lumley, J. L. 1965. Interpretation of time spectra measured in high intensity shear flows. *Phys. Fluids* 8: 1056–62

Lumley, J. L., Terray, E. A. 1983. Kinematics of turbulence convected by a random wave field. *J. Phys. Oceanogr.* 13: 2000–7

Lundgren, H. 1972. Turbulent currents in the presence of waves. *Proc. Coastal Eng. Conf., 13th,* pp. 623–34

Madsen, O. S. 1976. Wave climate of the continental margin: elements of its mathematical description. In *Marine Sediment Transport and Environment,* ed. D. J. Stanley, D. J. P. Swift, p. 602. New York: Wiley-Interscience

Madsen, O. S. 1977. A realistic model of the wind-induced Ekman boundary layer. *J. Phys. Oceanogr.* 7: 248–55

Madsen, O. S., Grant, W. D. 1977. Quantitative description of sediment transport by waves. *Proc. Coastal Eng. Conf., 15th,* 2: 1093–1112

Mellor, G. L., Yamada, T. 1974. A hierarchy of turbulence closure models for planetary boundary layers. *J. Atmos. Sci.* 31: 1791–1806

Miles, J. W. 1961. On the stability of heterogeneous shear flows. *J. Fluid Mech.* 10: 496–508

Miller, M. C., Komar, P. D. 1980a. Oscillation sand ripples generated by laboratory apparatus. *J. Sediment. Petrol.* 50: 173–82

Miller, M. C., Komar, P. D. 1980b. A field investigation of the relationship between oscillation ripple spacing and the near-bottom water orbital motions. *J. Sediment. Petrol.* 50: 183–91

Nielsen, P. 1981. Dynamics and geometry of wave-generated ripples. *J. Geophys. Res.* 86(C7): 6467–72

Niiler, P. P. 1975. Deepening of the wind-mixed layer. *J. Mar. Res.* 31: 405–22

Nowell, A. R. M. 1983. The benthic boundary layer and sediment transport. *Rev. Geophys. Space Phys.* 21(5): 1181–92

Nowell, A. R. M., Jumars, P. A., Eckman, J. E. 1981. Effects of biological activity on the entrainment of marine sediments. *Mar. Geol.* 42:133–53

Owen, P. R. 1964. Saltation of uniform grains in air. *J. Fluid Mech.* 20:225–42

Paradis, C. A. 1983. *Mechanics of sediment transport in the surf zone.* Masters thesis. Mass. Inst. Technol., Cambridge. 90 pp.

Perry, A. E., Schofield, W. H., Joubert, P. N. 1969. Rough wall turbulent boundary layers. *J. Fluid Mech.* 37:383–413

Rhoads, D. C., Boyer, L. F. 1982. The effects of marine benthos on physical properties of sediments. In *Animal-Sediment Relations*, ed. P. L. McCall, M. J. S. Teresz, pp. 3–57. New York: Plenum

Sanford, L. P. 1984. *The interaction of high frequency internal waves and bottom boundary layers on the continental shelf.* PhD thesis. Woods Hole Oceanogr. Inst./Mass. Inst. Technol., Woods Hole, Mass./Cambridge. 232 pp.

Smith, J. D. 1977. Modeling of sediment transport on continental shelves. In *The Sea*, Vol. 6, ed. E. D. Goldberg, I. N. McCave, J. J. O'Brien, J. H. Steele, pp. 539–77. New York: Wiley-Interscience

Smith, J. D., McLean, S. R. 1977a. Spatially averaged flow over a wavy surface. *J. Geophys. Res.* 82:1735–46

Smith, J. D., McLean, S. R. 1977b. Boundary layer adjustments to bottom topography and suspended sediment. In *Bottom Turbulence*, ed. J. C. J. Nihoul, pp. 123–51. New York: Elsevier

Soulsby, R. L. 1983. The bottom boundary layer of shelf seas. In *Physical Oceanography of Coastal and Shelf Seas*, ed. B. John, pp. 189–266. Amsterdam: Elsevier

Stefanick, T. A. 1979. *A realistic model of wave attenuation due to bottom friction.* SM thesis. Mass. Inst. Technol., Cambridge. 124 pp.

Swart, D. W. 1977. Predictive equations regarding coastal transports. *Proc. Coastal Eng. Conf., 15th*, 2:1113–32

Tennekes, H. 1973. The logarithmic wind profile. *J. Atmos. Sci.* 30:234–38

Thornton, E. B. 1979. Energetics of breaking waves within the surf zone. *J. Geophys. Res.* 84(C8):4931–38

Thorpe, S. A. 1985. A model of the turbulent diffusion of bubbles below the sea surface. *J. Phys. Oceanogr.* 14:841–54

Trowbridge, J. H. 1983. *Wave-induced turbulent flow near a rough bed: Implications of a time-varying eddy viscosity.* PhD thesis. Mass. Inst. Technol./Woods Hole Oceanogr. Inst., Woods Hole, Mass./Cambridge. 247 pp.

Trowbridge, J., Madsen, O. S. 1984a. Turbulent wave boundary layers. 2. Second order theory and mass transport. *J. Geophys. Res.* 89(C5):7999–8007

Trowbridge, J., Madsen, O. S. 1984b. Turbulent wave boundary layers. 1. Model formulation and first-order solution. *J. Geophys. Res.* 89(C5):7989–97

Weatherly, G. L., Martin, P. J. 1978. On the structure and dynamics of the oceanic bottom boundary layer. *J. Phys. Oceanogr.* 8(4):557–70

Weatherly, G. L., Van Leer, J. C. 1977. On the importance of stable stratification to the structure of the bottom boundary layer on the western Florida shelf. In *Bottom Turbulence*, ed. J. C. J. Nihoul, pp. 103–12. New York: Elsevier

Wiberg, P., Smith, J. D. 1983. A comparison of field data and theoretical models for wave-current interactions at the bed on the continental shelf. *Cont. Shelf Res.* 2:126–36

Wimbush, M., Munk, W. H. 1970. The benthic boundary layer. In *The Sea*, Vol. 4, ed. A. Maxwell, pp. 731–58. New York: Wiley-Interscience

Winant, C. D. 1980. Coastal circulation and wind-induced currents. *Ann. Rev. Fluid Mech.* 12:271–301

Wooding, R. A., Bradley, E. F., Marshall, J. K. 1973. Drag due to regular arrays of roughness elements of varying geometry. *Boundary-Layer Meteorol.* 5:285–308

Yaglom, A. M. 1979. Similarity laws for constant-pressure and pressure-gradient turbulent wall flows. *Ann. Rev. Fluid Mech.* 11:505–40

Zeman, O. 1981. Progress in the modeling of planetary boundary layers. *Ann. Rev. Fluid Mech.* 13:253–72